

誌謝

首先最要感謝的當然就是我的指導教授連正章博士，願意接納我這個半路出家、對神經電生理領域懷抱著過度理想憧憬的碩士生，引導我一步一步走進真正的神經生理學世界，也讓我下定決心將自己的青春歲月奉獻在浩瀚無垠的神經科學研究，毅然決然直升為博士生。在我漫漫的博士班生涯中，連博士除了帶領我一點一滴揭開大腦的神秘面紗之外，他以身作則地展現出對神經科學無比的熱忱以及對研究過程嚴謹的態度，甚至於對後生晚輩的悉心指教，在在都讓我深刻感受到這就是一個偉大無私的科學家典範。而我對於連博士特別感謝的是，在我坎坷曲折的博班研究旅程中，他一路扮演著披荊斬棘和激勵人心的先驅者，使我得以在經歷如此多刻骨銘心的挫折和痛苦後仍不放棄，最終在自己邁向科學家的路上能夠達到一個小小的里程碑。另外，我也感謝我碩班時的指導教授蔡惠珍博士，願意在我即將走投無路時收留我，教導我從事科學研究甚至於對待人生的基本觀念和態度，並放手讓我去追求自己的理想。我也感謝陳儀莊博士，讓我有機會抱著喜悅的心參與高水準的研究合作計畫。

感謝我博士學位口試委員們，閔明源博士、焦傳金博士、孫興祥博士、戴明泓博士、陳右穎博士、林惠菁博士、陳摘文博士以及林貝容博士等，為我在成為一個獨立研究人員的最後關頭嚴格把關，卻又避免澆熄我的科學研究的熱情，並且從不同思維角度提出獨特的見解，使我的博士論文得以更加完善。

感謝我實驗室的學長朱國彰，指導我電生理的技術及基本知識，讓我得以擁有雙手能自行摸索大腦的真面目。感謝實驗室的所有學長姐們，面惡心善的翁儒韻、勤奮執著的葉韋均、聰明伶俐的廖健璋、才貌兼俱的林晏竹和詹筑方，對我不管在實驗上或是生活上都照顧有加。感謝張敬邦學長在合作計畫上的努力及指教。感謝實驗室中跟我一起奮鬥到最晚的戰友吳僕射和侯文賢，少了他們，我應該很難撐過每一個漫漫的長夜。感謝學妹高敏華，在實驗上幫我了不少的忙。另外我也感謝實驗室的其他夥伴，劉予超、江柏翰、協助我達到畢業門檻的許燦庭、黃昱尹醫師、郭寧、郭子維、陳建錚、許至緯、謝育鳴、Ravi、陳彥竹、王凱誼、沈宏璋、認真負責的郭翊慧、洪明欣、謝瑀和王思懿、可愛又善解人意的哈比人陳亭仔、顏廷耘和陳玠汝、帥氣的曹茵綢和林昱伶、以及陪我舒展筋骨的陳勤霖，大家的共同努力奮鬥及陪伴豐富了我的知識及人生。

最後以及最重要的，我要感謝我在天上的母親，從小就對我無微不至的照顧及教導，使我能夠以樂觀進取的人生態度在這個世界上生存。感謝我的父親及哥哥，在遭逢如此大的變故之後，努力攬下家中的大小事務讓我得以專心完成博士學位。感謝游硯棋陪伴我渡過博班生涯早期及人生中最黑暗的時刻。感謝我的女友王姿文願意跟我一起走向充滿變數的將來。感謝我所有的朋友對我的支持和陪伴。

最後再次感謝所有曾經幫助過我或關心過我的人，在此表達最深切無盡的感激。

李政達

民國一〇四年七月十七日

ABSTRACT

The hippocampus plays a key role in learning and memory. The dentate gyrus (DG) serves as a gateway to the hippocampus, filtering and processing incoming afferent information from the cortex and passing output to other hippocampal areas. The DG comprises a heterogeneous population of neurons. Among them, granule cells (GCs), the largest neuronal population of the DG, are under tight inhibitory control by various types of GABAergic interneurons (INs) and thus display a high activation threshold. However, the causal link between identified GABAergic INs and GC activation in response to afferent activity from entorhinal inputs remains unknown. Here we show that pharmacological GABA_A receptor blockade not only greatly enhances the sensitivity of GCs to afferent inputs, but also recruits a subset of non-spiking GCs. Analysis of input threshold and spike timing of various types of GABAergic INs suggests that feedforward inhibition originating from somatic INs and molecular layer INs limits the dynamic range of input processing. Using cell type-specific optogenetic silencing, we found that parvalbumin-expressing (PV⁺) INs primarily suppress the population response of GCs to single-shock stimulation of cortical input. By contrast, PV⁺ and somatostatin-expressing (SST⁺) INs differentially regulate GC dynamics in response to θ and γ frequency inputs. Notably, PV⁺ INs control the onset of the spike series, whereas SST⁺ INs regulate the late spikes in the series. Together, these results demonstrate that specific types of GABAergic INs differentially regulate GC input transformations in response to different cortical input patterns.

中文摘要

海馬迴在學習與記憶上扮演著很關鍵的角色。而齒狀回就如同海馬迴的閘門，它負責過濾且處理從大腦皮質傳來的訊息，再將其傳遞至海馬迴其他的區域。齒狀迴是一個由許多不同種類的神經元所混雜組成的神經族群。而在這些神經元中，為數最多的顆粒細胞受到各種聯絡神經元嚴密的抑制性調控，因此具有很高的活化閾值。然而，對於目前已知的特定種類分泌伽瑪基丁酸的聯絡神經元在顆粒細胞被內嗅皮質傳來的訊息所活化時如何進行調控現在還不清楚。我們在此呈現的是以藥理學的方式將 A 型伽瑪基丁酸受器阻塞後，不只能大幅提升顆粒細胞對上游輸入的訊息的敏銳度，還能使多數在一般情況不產生動作電位的顆粒細胞被激活。從對齒狀回中各種分泌伽瑪基丁酸的聯絡神經元的輸入強度閾值及產生動作電位的時間點加以分析的結果可推測出，來自於針對細胞本體的聯絡神經元及分子層聯絡神經元的前饋抑制侷限了顆粒細胞所能處理上游輸入訊息的強度的動態範圍。利用針對特定種類細胞的光遺傳學活性抑制技術，我們發現表現小清蛋白的聯絡神經元是主要壓抑顆粒細胞對大腦皮質傳來的單一訊息所產生的群體反應的聯絡神經元。而相較之下，表現小清蛋白的聯絡神經元和表現生長激素抑制素的聯絡神經元會分別對顆粒細胞能處理西塔和伽瑪頻率的訊息輸入的動態範圍進行不同的調控。值得一提的是，表現小清蛋白的聯絡神經元負責調控一連串動作電位的開端，而表現生長激素抑制素的聯絡神經元則是負責調控一連串動作電位的後半段。總結來說，這些研究結果顯示出特定種類的聯絡神經元會對顆粒細胞在針對從大腦皮質傳來不同型式的訊息做訊息處理轉換時分別進行不同的調控。

TABLE OF CONTENTS

誌謝	i
ABSTRACT	ii
中文摘要	iii
TABLE OF CONTENTS	iv
ABBREVIATIONS	1
INTRODUCTION	3
The Hippocampus	3
The Dentate Gyrus	6
Inhibitory Circuits in the Dentate Gyrus	9
Signal Processing in a Neuron and in a Neuronal Population	13
The Arrangement of Axon Projection and the Dynamic Range in the Mammalian Brain	15
The Aim of This Study	17
MATERIALS AND METHODS	18
Electrophysiology	18
Calibration of Input Strength for GC Activation	20
Threshold Stimulation, Population Activation Curves, and Measurement of Excitatory and Inhibitory Postsynaptic Currents	21
Virus Injections	22
<i>Post-hoc</i> Recovery and Reconstruction of Recorded Neurons	23
Statistics	24
RESULTS	25
The GC Population Exhibit a Narrower Dynamic Range than the CA1 PC Population	25
Similar Inhibition-to-Excitation Ratios in the GCs	27
GABAergic Mechanism Restrains the Dynamic Range of the GC Population	28
Specific Types of GABAergic INs Restrict the Dynamic Range of the GC Population	30
Specific Types of INs Regulate I-O Transformations of the GC Population	32
PV ⁺ INs Constrain the Cortical Dynamic Range of the GC Population	33
PV ⁺ and SST ⁺ INs Differentially Regulate GC Population Spikes in the Series	34
DISCUSSION	37
Summary	37
Comparison to Previous Studies	37
The Definition of “Dynamic Range”	40
Shunting Inhibition Offsets GC I-O Relationships and Reduces Gain during Synaptic Excitation	41

A Lack of Synaptic Input Normalization in the GC Population	42
Bidirectional Regulation of Spike Timing by GABAergic Conductance in the DG GCs	43
Frequency-Tuned Distribution of Inhibition	43
REFERENCES	47
FIGURES AND TABLE	58
Fig. 1 Calibration of cortical input strength	58
Fig. 2 Isolation of monosynaptic EPSCs and feedforward IPSCs	59
Fig. 3 The granule cell (GC) population shows narrow dynamic range	60
Fig. 4 The dynamic range and gain of individual cells are not significantly different between the GC population and CA1 PC population	62
Fig. 5 Intrinsic properties of spiking and non-spiking GCs from adolescent rats	64
Fig. 6 Threshold excitatory inputs show no difference in GCs recruited at weak input or strong input	66
Fig. 7 The EPSTs are larger in CA1 PCs recruited at stronger input strength	68
Fig. 8 Threshold inhibitory inputs to the GCs recruited at weak input are similar to the GCs recruited at strong input	69
Fig. 9 Similar inhibition-to-excitation ratios in all recruited mature GCs	71
Fig. 10 GABAA conductance restricts the dynamic range of the GC population	72
Fig. 11 The dynamic range and gain of individual GCs are also modulated by GABAergic inhibition	75
Fig. 12 Regulation of the GC population dynamic range by somatic interneuron (INs) and ML INs	77
Fig. 13 Expression patterns of eNpHR3.0-eYFP in the ventral DG in cre-expressing mice	80
Fig. 14 Expression of eNpHR can selectively silence specific types of INs in DG	81
Fig. 15 Parvalbumin-expressing (PV ⁺) INs regulate GC input-output (I-O) transformations	83
Fig. 16 The lack of effect of silencing SST ⁺ INs on DG pSpike is not due to poor expression efficiency of NpHR-eYFP	85
Fig. 17 Silencing of PV ⁺ INs, but not SST ⁺ INs, expands the dynamic range of the GC population	86
Fig. 18 PV ⁺ and SST ⁺ INs differentially regulate the pSpike series in the GC population	89
Fig. 19 PV ⁺ and SST ⁺ INs differentially regulate the pSpike series in the individual GCs	91
Fig. 20 Calibration of cortical input strength from different recording sites in the same slice	92
Fig. 21 Intrinsic properties of spiking and non-spiking GCs from adult mice	94
Fig. 22 EPST negatively correlates with GC input resistance	96
Fig. 23 Comparison of functional properties between spiking (S) GCs and NS→S GCs, which transformed into spiking GCs after gabazine treatment	97

Fig. 24 GABAergic inhibition regulates spike latency in GCs_____98

Fig. 25 The GC input-output (I-O) transformations in optogenetic silencing of GAD65⁺ INs are comparable to that in gabazine_____99

CURRICULUM VITAE_____100



ABBREVIATIONS

AAC: axo-axonic cell

ACSF: artificial cerebral-spinal fluid

AP: action potential

BC: basket cell

DG: dentate gyrus

EC: entorhinal cortex

eNpHR: enhanced halorhodopsin

EPSC: excitatory postsynaptic current

EPSC_T: threshold excitatory postsynaptic conductance

fEPSP: field excitatory postsynaptic potential

GABA: γ -aminobutyric acid

GAD: glutamic acid decarboxylase

GC: granule cell

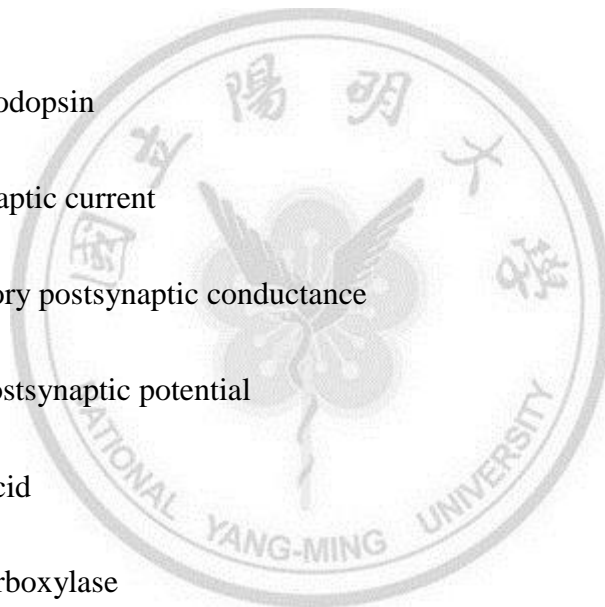
GCL: granule cell layer

HICAP: hilar commissural/association pathway-related

HIPP: hilar perforant pathway-related

IML: inner molecular layer

IN: interneuron



IPSC: inhibitory postsynaptic current

IPSG_T: threshold inhibitory postsynaptic conductance

LPP: lateral perforant pathway

MC: mossy cell

MLIN: molecular layer interneuron

MML: medial molecular layer

MOPP: molecular layer perforant pathway associated

MPP: medial perforant pathway

NGFC: neurogliaform cell

NS: non-spiking

OML: outer molecular layer

PC: pyramidal cell

PP: perforant pathway

pSpike: population spike

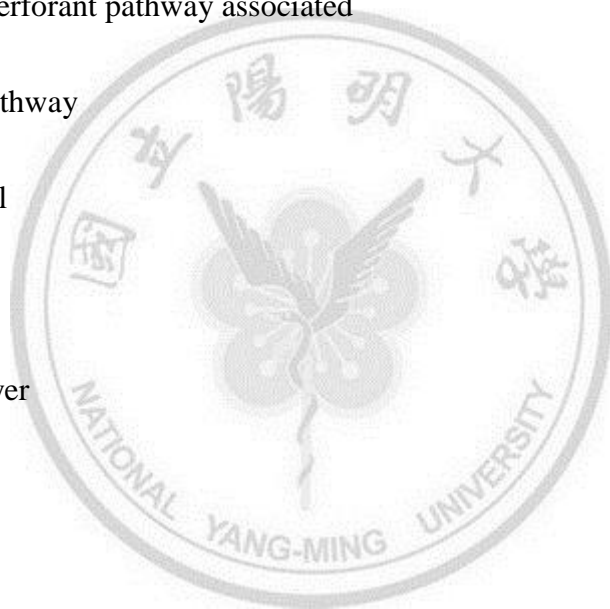
PV: parvalbumin

RMP: resting membrane potential

S: spiking

SST: somatostatin

TML: total molecular layer



INTRODUCTION

The Hippocampus

In 1564, Julius Caesar Aranzi, a Venetian anatomist, discovered a well laminated structure lying deep in the medial temporal lobes in the human brain and gave it a beautiful name according to its morphology, the “hippocampus”, which means the “seahorse” in Latin and originates from ancient Greek, ἵππος, "horse" and κάμπος, "sea monster". After that, the biologists found the same brain structures in other primates, mammals, or even birds successively (West 1990; Colombo and Broadbent 2000). In fact, evidence comes from neuroanatomical studies suggested that although the forebrain of vertebrates shows great variation in morphology, it still conserves a highly specialized structure, the hippocampus in birds and mammals or its homologue, the medial pallium in reptiles (Rodriguez et al. 2002). Furthermore, recent studies showed that either the hippocampus or medial pallium is likely an evolution of the pallial areas in the brain of teleost fish (Portavella et al. 2002; Jacobs 2003; Broglio et al. 2005; Vargas et al. 2006). No matter the hippocampus or medial pallium, although they come from various types of species, they are all critical for a basic survival requirement, the ability to encode spatial information and form cognitive representations of the environment (Rodriguez et al. 2002). However, with the progress of the evolution and changes of the environment, the cognitive functions of hippocampus become more and more complicated.

The earliest idea of hippocampal function in the mammals’ brain is about olfaction. It results from the anatomical studies about the projections of the hippocampus, lateral entorhinal cortex, and

olfactory bulb (van Groen and Wyss 1990). However, only a few specialists now believe that olfaction is the primary function of the hippocampus (Eichenbaum et al. 1991). Recently, there are two main thoughts about the hippocampal functions in mammals. The first one is called the Declarative Theory. This theory is mostly based on the pathological studies about patients with hippocampal damage. The most famous clinical report is about patient Henry Molaison (Patient H.M.; Scoville and Milner 1957). He received a surgery to remove bilateral hippocampus and most of entorhinal cortex in order to relief epileptic seizures. After that, although his epilepsy is under control, he suffered from severe anterograde and partial retrograde amnesia, especially in explicit memory, but his working memory and procedural memory remained intact. It is now widely accepted that the hippocampus play an important role in memory. The second theory is about spatial recognition. This theory is established by O'Keefe and Nadel and first supported by their study in 1971 (O'Keefe and Nadel 1978). In that study, O'Keefe and Dostrovsky discovered that principal neurons in the rat hippocampus show activities highly correlated to the rat's location within its environment (O'Keefe and Dostrovsky 1971). However, evidence for "place cells" in primates is relatively poor, probably due to the technical difficulties in recording brain activity from freely moving monkeys or human. Nevertheless, the same as the memory theory, it is now generally agreed that the hippocampus plays an important role in spatial coding.

Anatomical studies showed that, in mammals, the hippocampus receives signal inputs mainly coming from the entorhinal cortex (EC) and sends outputs back to the EC and other cortical areas

including prefrontal cortex (Amaral and Lavenex 2006). In addition to the EC, the hippocampus also receives modulatory inputs from the cholinergic neurons in the medial septal area, from the serotonin, norepinephrine, and dopamine systems (Amaral and Lavenex 2006). Since the hippocampus exhibits long, curved form across all mammalian orders, different regions along the longitudinal axis have different connectivities with cortical and subcortical areas and may also have distinct functions. Early lesion studies suggest that the dorsal (or posterior) hippocampus is associated to memory and spatial navigation, in contrast, the ventral (or anterior) hippocampus plays an important role in anxiety-related behaviors (Nadel 1968; Moser et al. 1993). However, accumulative evidence comes from gene expression studies, together with anatomical and electrophysiological studies indicate that there are functional long-axis gradients superimposed on discrete functional domains (Strange et al. 2014).

The hippocampus is composed by two main regions, the dentate gyrus (DG) and the Cornu Ammonis (CA; including CA1 to CA4). The central circuit in the hippocampus is called the trisynaptic circuit, which is initially described by the neuroanatomist Santiago Ramon y Cajal and is made up of DG granule cells (GCs), CA3 pyramidal cells (PCs) and CA1 PCs (Cajal 1893; Andersen et al. 1971 and 1975). The first synapse is formed by the axons from layer 2 of the EC (perforant pathway; PP) and the dendrites of DG GCs. The second synapse is composed of the mossy fibers, axons of DG GCs, and the proximal dendrites of CA3 PCs. The third synapse is made of schaffer collaterals, axon fibers from CA3 PCs, and dendrites of CA1 PCs. In addition to the trisynaptic circuit, there are some excitatory circuits also critical for hippocampal functions, for example, PP from layer

2 of the EC to CA3, PP from layer 3 of the EC to CA1, CA1 to subiculum, and feedback loop in the DG composed of SGC, GC, and hilar mossy cells (Larimer and Strowbridge 2010).

Because of the highly laminated structure and well organized arrangement of different types of neurons, the hippocampus is an excellent model system for studying neurophysiology such as synaptic transmission, synaptic plasticity, and intrinsic properties. Besides, in some common neurodegenerative disease and neurological disorders, for example, Alzheimer's disease, Huntington's disease, and temporal lobe epilepsy, the hippocampus is one of the most vulnerable brain regions and may play an important role in pathological process in these patients (Ransome et al. 2012; Moodley and Chan 2014). As a result, the hippocampus is a popular brain area for examining the pathogenic mechanisms or treatment strategies of these disease.

The Dentate Gyrus

Being the first relay station of the trisynaptic loop in the hippocampus, the DG serves as the gate keeper of the hippocampus. The dentate GCs receive massive inputs from layer 2 PCs of the EC and send rare but highly precise outputs to CA3 PCs (Acsády and Káli 2007). According to early anatomical studies, the DG performs a well laminated structure (Amaral et al. 2007). There are three layers, hilus, GC layer (GCL), and molecular layer (ML), from inside to outside of the DG (Cajal 1893). GCL is the primary location of the soma of principal excitatory neurons (GCs) in the DG. ML is where the apical dendrites of the GCs locate and where the first long-term potentiation has been

discovered (Bliss and Lomo 1973). In detail, ML can be divided into three parts, inner molecular layer (IML), medial molecular layer (MML) and outer molecular layer (OML). In general, IML represents the area that is covered by the axon fibers of hilar mossy cells (MCs) called commissural/associational pathway, and it is usually no more than 50 μm distant from GCL. In the middle third of ML, MML is mostly arborized by the axons from layer 2 PCs of medial EC called medial PP (MPP). Correspondingly, OML is about outer third of ML and occupied by lateral PP (LPP), axon fibers from layer 2 PCs of lateral EC. In the other side of GCL, hilus is not just the region that mossy fibers, the axons of GCs, pass through but also the location of cell bodies of hilar MCs and hilar INs.

The DG has two very unique properties compared to other brain areas. First, it is one of the only two regions existing adult neurogenesis in mammalian brains, even in the adult human brains there are more than 1400 new born GCs delivering to the DG everyday (Altman et al. 1965; Eriksson et al. 1998; Spalding et al. 2013). Although some evidence indicates that new born GCs may participate into preexisting DG circuits and have relatively high excitability to enforce synaptic transmission or synaptic plasticity, the exact physiological functions of these adult born GCs remain largely unknown (van Praag et al. 2002; Schmidt-Hieber et al. 2004; Marín Burgin et al. 2012). To examine the role of adult neurogenesis in cognitive functions, neuroscientists ablated the ability of neurogenesis in adult rodent brains and performed the behavioral tests, they found that ablated animals showed poor performance in pattern separation, spatial learning, and contextual fear conditioning, or vice versa

(Deng et al. 2010; Sahay et al. 2011; Denny et al. 2012). In addition, the first study using in vivo optogenetic manipulation of new born GCs showed that only silencing of 4-week-old adult born GCs during recall trials impaired spatial memories and contextual fear memories (Gu et al. 2012). However, more work needs to be done for understanding how new born GCs affect these cognitive functions. Second, only a little portion of GCs can be activated simultaneously by cortical inputs, which is called sparse coding (Chawla et al. 2005; Leutgeb et al. 2007; Tashiro et al. 2007; Alme et al. 2010). This unique coding scheme is considered to amplify small difference of upstream signals from the EC and send more distinguishable signals to the downstream CA3 region, and it is benefit for certain cognitive functions such as pattern separation (Aimone et al. 2011). The sparse coding predominately results from extremely passive membrane properties of the dendrites and somas in the DG GCs and powerful feedforward/feedback inhibitory circuits in the DG (Nitz and McNaughton 2004; Schmidt-Hieber et al. 2007; Ewell and Jones 2010; Krueppel et al. 2011; Dieni et al. 2013).

Since the DG has these specific properties, it attracts thousands of neuroscientists dedicating to understand its cognitive functions. Accumulating behavioral studies of animals with DG dysfunction showed that the DG plays an important role in spatial memory, pattern separation of similar objects, contexts, and odors (Kesner 2013). However, how DG contributes to hippocampal functions still remains to be clarified. For instance, the layer 2 PCs in the EC not only send signal outputs to the DG but also transmit the same signals to CA3. Furthermore, a single CA3 PC receives signals from only a few GCs (about 50) but from numbers of other CA3 PCs and layer 2 PCs, so how signals from the

DG GCs impact CA3 PCs remained unclear. In addition, the functions of DG GCs in rodents may not be the same as that in human according to several reasons. First, number of the DG GCs in human brains is about 10 fold of that in rodent brains, and the distribution of GC dendrites is also different between human and rodents. Second, human has much more complicated cognitive functions mediated by hippocampus, including formation or retrieval of episodic memory, compared to rodents. So far there is only a few studies examining the DG functions in the human brains, one of them using fMRI to show that pattern separation is correlated to DG/CA3 but not CA1/subiculum (Bakker et al. 2008). More efforts need to be devoted to explore the cognitive functions of the DG in human brains.

Inhibitory Circuits in the Dentate Gyrus

In mammalian brains, signal transmission from upstream to downstream region is mainly accomplished by excitatory neurons, but the activities of these neurons are tightly controlled by local inhibitory interneurons. In the single neuron level, the inhibitory interneurons not only determine whether these excitatory neurons are going to fire action potential or not, but also regulate the input-output gain and spike timing (Pouille and Scanziani 2001; Chance et al. 2002); while in the neuronal population level, the interneurons dominate the synchronized firing of whole population and determine the frequency of neuronal oscillations in different brain states (Whittington and Traub 2003; Dupret et al. 2008). There are two types of local inhibition in mammalian brains: tonic inhibition and phasic inhibition.

The first one mostly results from tonic activation of extrasynaptic GABA receptors induced by low concentration of ambient GABA in the microenvironment and is independent of neuronal activities (Farrant and Nusser 2005). Tonic GABA inhibition is first discovered in the cerebellum and then also found in other brain regions (Brickley et al. 1996; Nusser and Mody 2002; Semyanov et al. 2003). In the DG, high extracellular GABA levels generate a strong tonic inhibition in the GCs. The tonic inhibitory currents are mediated by δ subunit-containing extrasynaptic GABA receptors and are four times larger than spontaneous synaptic currents at about 10 Hz (Nusser and Mody 2002; Stell and Mody 2002). Therefore, the same as cerebellum, tonic inhibition plays a role in maintaining the DG in an extremely low activity state.

However, the predominant inhibition in the DG and other brain regions comes from the second type of inhibition, phasic inhibition (Farrant and Nusser 2005). Phasic inhibition means the rapid and transient inhibitory effects originate from the activation of synaptic receptors while local inhibitory interneurons are activated and release inhibitory neurotransmitters such as GABA and glycine (Curtis and Watkins 1960; Otsuka et al. 1966; Krnjevic and Schwartz 1967; Werman et al. 1967). As a result, the strength and timing of phasic inhibition is mediated by the activities of local interneurons. Although GABA conductance silences target neurons by hyperpolarizing membrane potentials in most cortical regions, it depolarizes membrane potentials in the DG GCs since the resting membrane potential is particularly negative (Staley and Mody 1992; Chiang et al. 2012). However, despite the depolarizing effects of GABA during resting state, GABA still inhibits the excitability of GCs in most

physiological conditions because the equilibrium potential of GABA receptors is much more negative than action potential threshold in the GCs, and this kind of inhibition is called shunting inhibition (Alger and Nicoll 1979; Andersen et al. 1980).

There are several forms of phasic inhibition in a neuronal network: feedforward inhibition, feedback inhibition, and lateral inhibition (Jonas and Buzsaki 2007). Feedforward inhibition indicates that when the excitatory signals come from upstream neurons, these signals may simultaneously activate target principal neurons and local inhibitory interneurons, and these interneurons will in turn send inhibitory signals to the principal neurons. Feedback inhibition means when the principal neurons are excited, they will also activate local inhibitory interneurons to inhibit themselves. Lateral inhibition is similar to feedback inhibition but the inhibitory targets are neighboring principal cells. These types of inhibition play specific roles in different brain states in DG (Ewell and Jones 2010).

In mammalian brains, most inhibitory interneurons innervate their axons to the specific subdomains of their target neurons (Somogyi et al. 1998). Hence in a well laminated brain structure such as hippocampus, the highly diverse local interneurons can be classified into several types according to the location of their somas and axonal arborization. In the DG, there are 6 types of interneurons according to this classification, basket cells (BCs), axo-axonic cells (AACs), hilar perforant pathway-related (HIPP) cells, hilar commissural/association pathway-related (HICAP) cells, total molecular layer (TML) cells, and molecular layer interneurons (MLINs) (Freund and Buzsaki

1996; Ramaswamy 2015). Recently, MLINs has been divided into two types, molecular layer performant path-associated (MOPP) cells and neurogliaform cells (NGFCs), according to their biomarkers, membrane properties, and synaptic properties (Halasy and Somogyi 1993; Armstrong et al. 2011). All these interneurons directly target GCs and play different roles in feedforward, feedback, and lateral inhibition (Liu et al. 2014). In addition to direct GC inhibition, several types of interneurons also innervate other interneurons resulting in disinhibition or synaptic modulation, which subsequently modulates signal transformations in the GC population (Földy et al. 2007; Liu et al. 2014; Savanthrapadian et al. 2014). Since the unique axonal arborizations, fast spiking properties, and high excitability to their afferents are easy to be recognized, BCs become the well-studied interneurons in the DG (Geiger et al. 1997; Ewell and Jones 2010). Previous studies show that DG BCs play critical roles in gamma oscillation, which is generated in the DG and linked to memory and “conscious” experience (Fell et al. 2001; Varela et al. 2001; Pöschel et al. 2002; Csicsvari et al. 2003; Bartos et al. 2007) . And they are also closely related to several neural disorders such as epilepsy and Alzheimer’s disease (Sloviter et al. 1991, 2003; Ribak 1992; Brady and Mufson 1997). However, functions of other types of DG interneurons under physiological or pathological conditions are largely unknown. Recently, neuroscientists have some progress in understanding how DG interneurons regulate the response of the GCs to the cortical inputs depending on several indirect evidence. For instance, since perisomatic targeting interneurons such as BCs and AACs can easily be recruited by initial PP and C/A activities and show multiple pulse depression, they are considered as the detectors

of the onset of a series of upstream activities and regulate the initial response of the GCs (Ewell and Jones 2010; Sambandan et al. 2010; Liu et al. 2014). Whereas dendritic targeting interneurons such as HIPP and HICAP cells are relatively reactive to GC activities compared with PP or C/A activities and shows multiple pulse facilitation, therefore these interneurons are thought to detect and regulate GC response in the late phase of activity series (Hosp et al. 2014; Liu et al. 2014). However, these hypotheses still remain to be proved by direct evidence.

Signal Processing in a Neuron and in a Neuronal Population

To keep surviving in this world, animals have to respond appropriately to volatile changes of the surrounding environment, therefore, they require a structure which can integrate lots of sensory inputs and make final decisions after a series of computation. And after billions of years of evolution, the central nervous system, brain, has become a highly specialized structure which is optimized for complicated computation, especially in human (Hofman 2014). As a result, understanding how the brain processes various signals is always an important and challenging issue. Compared to the complex connections between billions of neurons in a brain, a single neuron has long been considered as a simple linear summation and thresholding device of a neural network by most computational neuroscientists (McCulloch and Pitts 1943). However, accumulative evidence show that an individual neuron can do complex arithmetic operations through their unique biophysical mechanisms (Hoffman et al. 1997; Golding and Spruston 1998; Silver 2010; Hu et al. 2014). Most neurons receive upstream signals at dendritic spines, which in term propagate signals along the highly branched dendrites to the

soma for integration, and these integrated signals subsequently trigger action potentials in the axon initial segment and output to downstream targets by synaptic transmission (Cajal 1933). In fact, according to recent studies, signals has already been fully processed before they reach soma (Cash and Yuste 1999; Schmidt-Hieber et al. 2007; Krueppel et al. 2011). At dendritic spines, NMDARs can amplify larger or temporally coincident signals from others, and short term plasticity may also regulates the strength of temporally associated signals but remains independent signals unchanged (Rothman et al. 2009; Zheng and Rusakov 2015); on dendrites, signals from spatially segregated or spatially clustered synapses can be differentially affected by synaptic noise, shunting conductance, and nonlinear dendritic conductance such as voltage gated Na^+ channels, Ca^{2+} channels, A type K^+ channels, which may all enlarge the difference and help soma to discriminate spatial and temporal correlations in these signals (Hoffman et al. 1997; Golding and Spruston 1998; Cash and Yuste 1999; Doiron et al. 2001; Mitchell and Silver 2003; Kampa and Stuart 2006; Losonczy and Magee 2006). A single neuron can encode signals in one of at least two ways: firing rate as an integrator or correlations in spike timing as a coincidence detector (Adrian and Zotterman 1926; Vinje and Gallant 2000; Olshausen and Field 2004). The offset and gain of the input-output relationship in both ways of neuronal coding are determined by signal processing in dendritic spines, dendrites, and soma, and affected by various biophysical mechanisms in multiplicative/divisive or additive/subtractive ways (Silver 2010).

In mammalian brain circuits, neurons responsible for the same cognitive functions cluster

together to form neuronal populations or neuronal assemblies, and these neuronal populations may process and encode complicated information from upstream brain regions and send outputs to downstream target regions (Georgopoulos et al. 1986; Buzsaki 2010). As a result, how signals are encoded or processed in a neuronal population is also an important question (Sakurai 1999). The input-output transformation of a neuronal population is not only determined by the individual principal neurons but also largely affected by different connections and synaptic properties between various types of local neurons and between upstream neurons and these local neurons (Pouille et al. 2009). In the DG, although plenty of studies indicate that GC population perform sparse population coding and it is primary determined by powerful GABAergic inhibition (Ewell and Jones 2010; Dieni et al. 2013; Yu et al. 2013). However, the underlying cellular mechanisms of this inhibition and the input-output relationship of GC population remain unclear.

The Arrangement of Axon Projection and the Dynamic Range in the Mammalian Brain

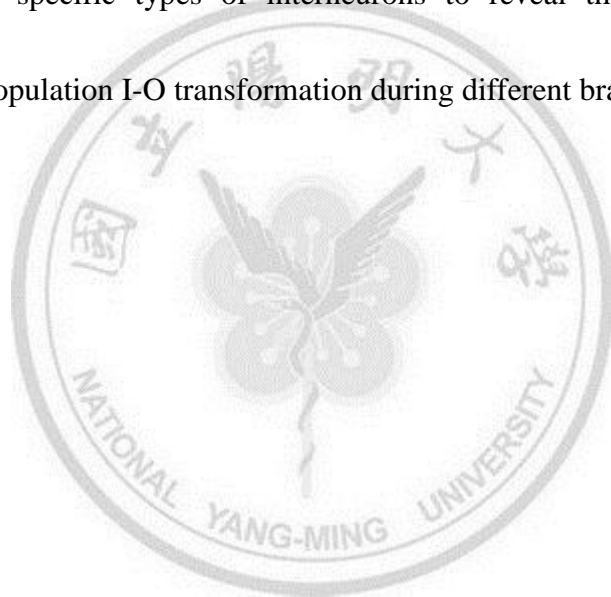
Cortical excitatory neurons project their axons in an extremely divergent and convergent manner (Tamamaki and Nojyo 1993; Chklovskii 2004; Dancause et al. 2005), making them capable of communicating with multiple postsynaptic neurons and allowing individual postsynaptic neurons to receive inputs from many presynaptic neurons (van Groen et al. 2003). This arrangement allows cortical neurons to process complex computations during cognitive behaviors. However, in such a circuit, small fluctuations in the proportion of neurons that are presynaptically active (note that the number of active neurons is also referred to as the input strength) elicits all-or-none recruitment of

the entire postsynaptic population (Pouille et al. 2009). Thus, without specific control mechanisms, small changes in presynaptic neuronal activity may cause all-or-none activation of the postsynaptic neuronal population (Marr 1969; Shadlen and Newsome 1998; Diesmann et al. 1999; Vogels and Abbott 2005).

Neuronal circuits in different brain regions have distinct strategies to prevent this ‘all-or-none’ predicament. In the rodent hippocampal CA1 region and somatosensory cortex, global feedforward inhibition can elevate the threshold for excitatory currents in postsynaptic PCs as presynaptic input strength increases, thereby expanding the range of input strengths (i.e., the dynamic range) that neuronal populations can represent (Pouille et al. 2009). In the hippocampal formation, EC innervation of GCs, the principal cells of the dentate gyrus (DG) exhibits massive convergence and divergence (Tamamaki and Nojyo 1993; van Groen et al. 2003). Such massive divergent and convergent excitatory innervation places the GC population at a serious risk of ‘all-or-none’ activation, as outlined above. Surprisingly, under physiological conditions only a small proportion (1–2%) of the GC population can be activated simultaneously by a barrage of excitatory inputs from the EC and relay cortical signals to the downstream CA3 region (Chawla et al. 2005; Tashiro et al. 2007; Alme et al. 2010). Although inhibition within the DG circuits originating from multiple GABAergic IN populations is a prime mediator of the sparse activation of GCs (Acsády and Káli 2007; Coulter and Carlson 2007; Ewell and Jones 2010; Dieni et al. 2013; Yu et al. 2013), the causal role of specific types of GABAergic INs in this signal processing remains unclear.

The Aim of This Study

In this study, we aim to explore the role of specific types of interneurons in the DG during signal processing. First we examine the cortical dynamic range of the GC population during sparse activity and compare with that of CA1 pyramidal cell population by using slice electrophysiology. Then we investigate the effects of GABAergic inhibition on the dynamic range and the underlying cellular mechanisms combining pharmacology, immunostaining and electrophysiology. Finally, we perform optogenetic silencing of specific types of interneurons to reveal the impacts of these local interneurons on the GC population I-O transformation during different brain states.



MATERIALS AND METHODS

Electrophysiology

Transverse ventral hippocampal slices (350–400 μm) were prepared from the brains of male Sprague-Dawley rats (3–4 weeks) or C57BL/6 mice (3–6 months). For optogenetic experiments, transgenic hemizygote mice (2–4 months) of either sex were used. *Gad65-cre* (also known as *Gad2-cre*), *Pvalb-cre*, *Sst-cre* (also known as *Som-cre*), and *Ai14* reporter mice were obtained from the Jackson Laboratory (stock nos 010802, 008069, 013044, 007914, respectively; The Jackson Laboratory, Bar Harbor, ME, USA) and maintained on the C57BL/6J background. Slices were sectioned in carbogen (95% O₂ and 5% CO₂) bubbled ice-cold artificial CSF (ACSF) containing (in mM): 125 NaCl, 25 NaHCO₃, 1.25 NaH₂PO₄, 2.5 KCl, 25 glucose, 2 CaCl₂, and 1 MgCl₂, and recovered (25 min, 34°C) in modified oxygenated ACSF containing (in mM): 87 NaCl, 25 NaHCO₃, 2.5 KCl, 10 glucose, 75 sucrose, 0.5 CaCl₂, and 7 MgCl₂ before transferring to standard oxygenated ACSF. Slices were placed in a submerged chamber and superfused with oxygenated ACSF (32 \pm 1°C) during experiments. All experiments were conducted in accordance with methods approved by the Animal Care and Use Committee of National Yang-Ming University.

GCs and INs in the DG were visually identified using infrared Dodt gradient contrast microscopy. Cell-attached and whole-cell recordings were performed using patch pipettes (with a resistance of 8–10 M Ω and 4–6 M Ω , respectively) filled with internal solution, consisting of (in mM): 146.5 potassium gluconate, 3.5 KCl, 1.5 MgCl₂, 5 HEPES buffer, 1.1 EGTA, 2 Na₂ATP, and 10

phosphocreatine (pH = 7.3, 295–305 mOsm). Series resistance was not compensated but was monitored continuously throughout the recording. Recordings with series resistance < 30 MΩ were analyzed. All experiments were performed in the presence of the *N*-methyl-D-aspartate (NMDA) receptors antagonist D-AP5 (20 μM) and the GABA_B receptor antagonist CGP55845 (1 μM). Pharmacological blockade of NMDA receptors and GABA_B receptors is to prevent synaptic plasticity at excitatory inputs and disinhibition of GABAergic transmission during experiments. Slices containing the ventral DG were selected for experiments because the PP projection from the EC can be largely preserved in the subiculum in this preparation. The PP fibers were stimulated for 0.1 ms with constant current (range of 10–1000 μA) using a monopolar electrode placed in the subiculum to avoid the direct activation of axons from DG INs. Loose-patch recordings were performed with patch pipettes (of resistance 6–10 MΩ) filled with ACSF. Field recordings were performed also with ACSF-filled patch pipettes (with a resistance < 1 MΩ). Signals were recorded with Multiclamp 700B amplifiers (Molecular Devices). Data were filtered at 2 kHz and sampled at 10 kHz with a Digidata 1440 interface (Molecular Devices) controlled by pCLAMP 10.2 software (Molecular Devices). For optogenetic silencing of eNpHR3.0-expressing neurons, amber light was emitted from a collimated light-emitting diode (590 nm) driven by a 4 channel LED Driver (Thorlabs) under the control of a Digidata 1440A and Clampex 10.2. Light was delivered through the reflected light fluorescence illuminator port and the ×63 objective. Kynurenic acid (KA, 2 mM) and gabazine (1 μM) were used to block ionotropic glutamate receptors and GABA_A receptors, respectively.

Calibration of Input Strength for GC Activation

The input strength was calibrated in all experiments as described previously (Pouille et al. 2009). Briefly, the input strength is a value that represents the number of active presynaptic neurons and is normalized from 0 to 1, permitting the comparison of stimulus intensities across slices. We used two parameters to calculate the input strength: the initial slope (20–50%) of the field excitatory postsynaptic potential (fEPSP), which is proportional to the number of activated PP fibers, and the area under the population spike (pSpike), which is proportional to the number of active GCs around the DG recording sites (Fig. 1). Therefore, all the input strengths shown in this study were performed in the presence of two field recording electrodes: one placed in the ML, for fEPSPs, and one in the GC layer (GCL), for pSpikes. The fEPSP slope evoked at any given stimulus intensity was normalized to the fEPSP slope elicited by a stimulus intensity that resulted in a pSpike at 95% of its maximum (which means 95% of local spiking GCs are recruited). The value of such normalized fEPSP is the input strength. Thus, an input strength of 1.0 means that the number of stimulated PP fibers can recruit 95% of local spiking GCs and an input strength of 0.1 means that the number of stimulated PP is one-tenth of the number at input strength 1.0. For each slice, the input strength was determined under control conditions. Therefore, the number of PP fibers stimulated in control conditions, or in the presence of gabazine, was the same for a given input strength within a slice. The amplitude of the pSpike had to remain stable for at least 10 min before the input strength was calibrated.

Threshold Stimulation, Population Activation Curves, and Measurement of Excitatory and Inhibitory Postsynaptic Currents

Neurons were recorded in the loose-patch or cell-attached configuration, and the PP stimulated at different intensities to determine the threshold input strength, which evoked a 50% of maximum spike in the recorded cells. After determining the threshold input strength, neurons were subsequently re-patched with a pipette containing internal solution, to achieve whole-cell patch recordings. In a subset of the recordings, we determined threshold input strength in the whole-cell recording configuration. The threshold input strength did not differ notably from the one obtained in the loose-patch or cell-attached configuration, so results from all GC recordings were combined.

The population activation curve is the cumulative distribution of the input strength which evokes 50% spiking probability in the neurons in that population. Five to ten stimuli were tested at each intensity to calculate spiking probability. The 50% spiking probability of individual neurons was determined by fitting their spiking probability plotted against input strength with a sigmoid function $Y = 100/[1+10^p(x_0-x)]$, where x_0 is the input strength at 50% spiking probability, and p is the slope at x_0 . PP-fiber stimulation evoked an excitatory postsynaptic current (EPSC)–inhibitory postsynaptic current (IPSC) sequence in GCs voltage-clamped at -55 mV (Fig. 2). To confirm that recorded IPSCs resulted from the synaptic activation of GABAergic INs but not direct stimulation of inhibitory axons, we only considered experiments in which IPSCs could be abolished by the ionotropic glutamate receptor antagonist KA (resulting in at least a 70% reduction; Fig. 2B). EPSCs were isolated by

voltage clamping the GCs at the reversal potential of the IPSC (-75 mV). To estimate the amplitude of the EPSCs recorded at -55 mV, we used the amplitude of the EPSC recorded at the reversal potential of the IPSC after scaling its initial slope to the initial slope of the EPSC recorded at -55 mV (Fig. 2B).

The feedforward/feedback IPSC was isolated by subtracting the scaled EPSC from the EPSC-IPSC sequence (recorded at -55 mV). To eliminate the contamination of IPSCs resulting from direct IN activation, the remaining IPSCs recorded in the presence of KA were also subtracted from the EPSC-IPSC sequence. EPSC and IPSC were calculated from the respective peak currents, assuming ohmic behavior and reversal potentials of 0 and -75 mV (Fig. 2B).

Virus Injections

To selectively silence genetically defined INs in the DG, we used an AAV5 carrying a Cre-inducible eNpHR3.0-eYFP transgene (AAV5-EF1 α -DIO-eNpHR3.0-eYFP) (for most experiments) or an AAV5 carrying Cre-inducible eNpHR3.0-mCherry (remaining experiments), both of which were produced by the University of North Carolina Vector Core Facilities, Chapel Hill, NC, USA. Mice (postnatal day > 45) were anesthetized with 4% isoflurane (vol/vol; Halocarbon Laboratories, North Augusta, SC, USA) in 100% oxygen in an induction chamber (air flow rate: 4 mL/min), and their heads were shaved for craniotomy. The mice were placed into a stereotaxic frame (Stoelting Co., Wood Dale, IL, USA) and anaesthesia was maintained with constant 1.5% isoflurane air flow (4 mL/min). A homeothermic blanket (Panlab Harvard apparatus, Barcelona, Spain) was placed under the

mice to keep the body temperature constant (34°C). The surgical area was sterilized using 75% ethanol and the eyes were protected using ophthalmic gel. For targeting DG INs of the ventral hippocampus, a midline scalp incision (~1 cm) was made with scissors and the skin pulled aside to expose the skull. A small craniotomy (coordinates from bregma were as follows: anteroposterior, -3.4 mm; mediolateral, ±2.8 mm) was made at the hypothetical intersecting point on the skull, through which an imaginary vertical axis connects the craniotomy and the targeted areas in the underlying ventral hippocampus. The viral vector was delivered through the craniotomy to two locations within the ventral hippocampus (coordinates: anteroposterior, -3.4 mm; mediolateral, ±2.8 mm; dorsoventral, -4.4 mm and -4.2 mm), using a 10 µL NanoFil syringe (World Precision Instruments, Sarasota, FL, USA) and a 35-gauge beveled metal needle. Injection volume (0.5 µL at each location) and flow rate (0.1 µL/min) were controlled with a Nanopump Controller (KD Scientific, Holliston, MA, USA). After injection, the needle was left in place 0.2 mm above the injection site for 10 min before slow withdrawal. Following suturing of the craniotomy, mice were placed back in the home cage for recovery. All animals were allowed to recover for at least 6 weeks before the next experimental stage, to ensure complete recovery from surgery and to allow gene transduction.

***Post-hoc* Recovery and Reconstruction of Recorded Neurons**

Recorded GCs and INs were filled with biocytin (0.4%) during whole-cell recordings and subsequently fixed overnight with 4% paraformaldehyde in phosphate-buffered solution (PBS; 0.1 M, pH 7.3). After washing with PBS, slices were incubated with fluorescein isothiocyanate (FITC)-

conjugated avidin-D (2 μ l/ml; Invitrogen) in PBS and 0.3% Triton X-100 overnight at 4°C. After washing, slices were embedded in Vectashield mounting medium (Vector Laboratories). Labeled cells were imaged by two-photon microscopy and reconstructed with Neuromatic 1.6.3 software (Myatt et al. 2012).

Statistics

Average values are expressed as means \pm standard error of mean (s.e.m.). Error bars in the figures also indicate s.e.m. (shown only if larger than symbol size). Statistical significance was tested by the Wilcoxon signed-rank for paired data or Wilcoxon rank-sum test for unpaired data at the significance level (p) as indicated using Prism 5.0 (GraphPad Software, La Jolla, CA, USA). We used two-way repeated measures of ANOVA to compare the effects of IN silencing on GC population activity at different input strengths or input frequencies. Statistical significance of linear regressions was tested by F-tests.

RESULTS

The GC Population Exhibit a Narrower Dynamic Range than the CA1 PC Population

Feedforward GABAergic inhibition in the CA1 area is shown to expand the range of afferent input strengths that a neuronal population can represent (Pouille et al. 2009). However, we know that activation of individual GCs in response to cortical inputs is primarily restrained by powerful GABAergic inhibition (Ewell and Jones 2010; Marín-Burgin et al. 2012; Dieni et al. 2013). What is the net effect of GABAergic inhibition on the dynamic range of the GC population in response to cortical inputs? We first sought to establish the cortical range which the GCs represents, and compare it with that of the CA1 PC population in acute brain slices from 3- to 4-week-old rats. For this, we stimulated the cortical inputs, the medial (MPP) and lateral (LPP) PPs, by placing a stimulation electrode on the subicular side (Sub) of the hippocampal fissure (Fig. 3A). While stimulating, we simultaneously recorded action currents ('spikes') in the cell-attached configuration from individual GCs located in the middle and outer thirds of the GCL, along with the corresponding fEPSPs, over a range of stimulus intensities (Fig. 3A). The spiking probability of individual GCs increased while increasing stimulus intensities. To establish the activation profile of single GCs, we plotted the spiking probability against input strength (for calibration of input strength, see Fig. 1 and Pouille et al. 2009) and fitted them with a sigmoid function (Fig. 3B; see Materials and methods). We next defined the threshold input strength as the input strength which could evoke 50% spiking probability in individual GCs. Comparable with previous studies (Chawla et al. 2005; Marín-Burgin et al. 2012),

47% (62 of 131) of recorded GCs could be recruited ('spiking GCs') in this stimulating paradigm (Fig. 3C, 'S' in the pie chart).

Following cell-attached recordings, we made whole-cell recordings from the same cells and determined their input resistance. The input resistance was measured by the ratio of the steady-state (average of the last 100 ms) voltage response versus the injected 1-s hyperpolarizing (20 or 50 pA) current pulse. In the present study, GCs with input resistance $\leq 0.5 \text{ G}\Omega$ were classified as mature GCs, and about 98% of spiking GCs were mature GCs (data not shown, Dieni et al. 2013). A cumulative distribution of threshold input strengths from all spiking GCs was used to build the population activation curve, which represents the fractional recruitment of the GC population as a function of the input strength ($n = 62$ cells; Fig. 3C, E). The dynamic range of the GC population (the ratio of the input strengths that activate 95% versus 5% of the spiking GC population) was approximately 3.5 (Fig. 1E), meaning that the GC population has the ability to distinguish and respond to only a 3.5-fold increase in the number of active PP inputs before saturating. This is much smaller than the input range of the CA1 PC population examined in the same way, which was approximately 16 ($n = 44$ cells; Fig. 3D, E, 7A). The histogram of threshold input strength also showed that spiking GCs were recruited by an input strength of more than 0.2 (Fig. 3F); whereas CA1 PCs were recruited through a wide range of input strengths (from 0 to 1; Fig. 3G).

Whereas the dynamic range of the GC population was much smaller than that of the PC

population, the dynamic range of individual GCs (1.36 ± 0.03 , $n = 48$; Fig. 4A, B) was not significantly different from that of PCs (1.44 ± 0.05 , $n = 27$; Fig. 4A, B) throughout the threshold input strength from 0 to 1. Similarly, there is also no significant difference between GCs and PCs in the gain, defined by the slope factor of the sigmoidal fit (GC, 20.38 ± 1.46 , $n = 48$ versus PC, 37.45 ± 10.07 , $n = 27$; $p = 0.09$; Fig. 4C, D).

Similar Inhibition-to-Excitation Ratios in the GCs

Several factors influence the dynamic range of a neuronal population such as intrinsic properties of individual neurons, extrinsic inputs, and other neuromodulators (Shu et al 2003; Carvalho and Buonomano 2009; Pouille et al. 2009). Analysis of the functional properties of all spiking GCs, including input resistance, resting membrane potential (RMP), membrane time constant (τ), and action potential (AP) threshold of individual GCs showed no correlation with the threshold input strength although most of them (input resistance, membrane τ , and AP threshold) were significantly different in spiking GCs and non-spiking GCs (Fig. 5).

Next, we examined the excitatory and inhibitory synaptic inputs evoked by PP stimulation. By either simultaneously or sequentially making dual recordings, we established the threshold input strengths of two individual GCs and then recorded the threshold EPSCs (EPSC_{Ts}) and concomitantly triggered threshold IPSCs (IPSC_{Ts}) in voltage clamp (Fig. 6A, 8A). EPSCs were recorded in the GCs at -75 mV, which was close to the reversal potential of the IPSC. To estimate the amplitude of the

EPSCs recorded at -55 mV, we scaled the initial slope (20%-50%) of the EPSC recorded at -75 mV to that of the EPSC recorded at -55 mV (Fig. 2). The IPSC was isolated by subtracting the scaled EPSC from the EPSC–IPSC sequence recorded at -55 mV (Fig. 2). Threshold excitatory conductance (i.e., $EPSC_{T}$) and threshold inhibitory conductance (i.e., $IPSC_{T}$) were calculated from their respective peak currents (see Materials and methods). There was no correlation between the $EPSC_{T}$ s and threshold input strengths ($n = 47$, $R^2 = 0.05$, $p = 0.65$; Fig. 6B), which was quite different from observations of CA1 PCs, in which the PCs recruited at higher input strengths require larger $EPSC_{T}$ s (Fig. 7B; also see Pouille et al. 2009). Also, $EPSC_{T}$ s from the GCs recruited by weak input are similar to that from the GCs recruited by strong input (Fig. 6C). And neither did the $IPSC_{T}$ s correlate with the threshold input strengths ($n = 39$, $R^2 = 0.11$, $p = 0.47$; Fig. 8B). Although $IPSC_{T}$ s from the GCs recruited by strong input mostly exhibited large values than that from the GCs recruited by weak input in the same slices, there is no significant difference between them ($n = 7$ pairs, $p = 0.22$; Fig. 8C). However, the $IPSC_{T}$ s positively correlated with the $EPSC_{T}$ s ($n = 35$, slope = 1.02; $R^2 = 0.4$, $p < 0.0001$; Fig. 9A), yielding similar inhibition-to-excitation ratios in all spiking GCs and they were independent of threshold input strength (Fig. 9B). This consistency of inhibition-to-excitation ratios in the same neuronal population were also observed in other brain regions (Pouille et al. 2009; Xue et al. 2014).

GABAergic Mechanism Restrains the Dynamic Range of the GC Population

Unlike CA1 PCs, GCs were insensitive to input strengths of less than 0.2. What makes the GCs

refractory to weak inputs? GABAergic inhibition (whether hyperpolarizing or shunting) is known to offset the neuronal I-O relationship (Chance et al. 2002; Mitchell and Silver 2003; Marín-Burgin et al. 2012). To confirm this, we first compared the timing of the spike elicited in GCs by PP stimulation with the onset of the IPSC. When stimulated at the threshold for spike generation, the spike occurred 5.30 ± 0.18 ms after the onset of the EPSC and 2.13 ± 0.23 ms after the onset of the IPSC ($n = 18$; Fig. 10A). The latency between the onset of the EPSC and IPSC was 3.17 ± 0.22 ms ($n = 18$). Thus, in response to threshold PP stimulation, inhibition impinged on GCs before the membrane potential of the neuron reached the threshold for spike generation, thereby offsetting the I-O relationship. Consistently, we found that complete removal of GABAergic inhibition with the GABA_A receptor antagonist gabazine ($1 \mu\text{M}$) increased the spiking probability of individual GCs with the same input strength (Fig. 10B) and induced a significant reduction in the threshold input strength required to activate GCs ($n = 10$, $p < 0.01$; Fig. 10C). In addition to the reduction of threshold input strength, gabazine also transformed a subpopulation of non-spiking (NS) GCs into spiking GCs ($n = 10$, dashed lines; Fig. 10D). By decreasing the threshold input strength of spiking GCs and recruiting most non-spiking GCs, gabazine greatly expanded the dynamic range of the GC population (control, 3.5-fold; gabazine, 8-fold; Fig. 10E). The bimodal distribution of threshold input strengths after gabazine treatment also suggested that there were two GC subpopulations, one with high-threshold, which mostly comes from spiking GCs in control condition, and one with low-threshold input strength coming from non-spiking GCs in control condition (Fig. 10F, G).

In contrast to its effect on GC population, gabazine treatment robustly decrease the dynamic range of individual GCs (control, 1.36 ± 0.03 versus gabazine, 1.27 ± 0.03 ; $n = 49$ versus 27 , $p < 0.01$; Fig. 10A, B). Similarly, it also significantly increased the gain of individual GCs (control, 20.38 ± 1.46 versus gabazine, 37.67 ± 5.62 ; $n = 49$ versus 27 , $p < 0.01$; Fig. 10C, D). These results demonstrate that GABAergic inhibition limits the dynamic range of the GC population by elevating the input threshold of spiking GCs as well as by restraining a large population of GCs from spiking in response to PP stimulation. And the results also confirmed that the dynamic range of the GC population is not determined by the dynamic range of individual GCs.

Specific Types of GABAergic INs Restrict the Dynamic Range of the GC Population

Various types of GABAergic INs in the DG serve distinct inhibitory roles (Freund and Buzsáki 1996; Hájos et al. 1996; Boyett and Buckmaster 2001; Bartos et al. 2002; Armstrong et al. 2011; Kullmann 2011; Li et al. 2013; Liu et al. 2014). Which types of INs are involved in regulation of spike probability of individual GCs triggered by single-shock stimulation of the PP and consequently limit the dynamic range of the GC population? To affect GC spiking, these INs must discharge before GCs in response to PP stimulation and need to have a relatively low threshold input strength (Pouille et al. 2009). Here we examined the spiking of several distinct IN types in response to averaged threshold PP stimulation of GCs (i.e., 0.5 input strength) and compared their spike timing with GCs (Fig. 12A–I). According to the target selectivity of the axon, somatic locations, and physiological properties (Armstrong et al. 2011; Hosp et al. 2014; Liu et al. 2014), we identified seven distinct subclasses of

INs: basket cells (BCs) and axo-axonic cells (AACs), which are both fast spiking perisomatic targeting INs; hilar PP-associated (HIPP) cells, hilar commissural–associational pathway related (HICAP) cells, and total molecular layer (TML) cells, which all target dendrites of the GCs so called dendritic INs; ML PP–associated (MOPP) cells and neurogliaform cells (NGFCs), their soma are both located in the ML thus termed ML INs. In these seven types of INs, somatic INs (including BCs and AACs; BC/AAC in figures), MOPP cells, and NGFCs spiked earlier than GCs (somatic INs, -3.09 ± 0.28 ms, $p < 0.001$, $n = 14$; MOPP cells, -2.82 ± 0.38 ms, $p < 0.001$, $n = 7$; NGFCs, -2.91 ± 0.64 ms, $p < 0.001$, $n = 9$; Fig. 12I for the summary); whereas only two of TML ($n = 2/4$; Fig. 12F) cells could be recruited by near maximal stimulation, and neither HIPP ($n = 6$; Fig. 12D) nor HICAP cells ($n = 7$; Fig. 12E) were recruited by the maximal input stimulation (i.e., 1.0 input strength). In addition to the spike timing, various types of INs showed distinct input thresholds. Analysis of activation curves from all recorded INs revealed that most of somatic INs ($n = 12/14$) and all of MOPP cells ($n = 7/7$) and the majority of NGFCs ($n = 6/10$) were recruited by PP stimulation below an input strength of 0.2, at which non GCs were recruited ($n = 0/62$; Fig. 12J). By contrast, no HIPP or HICAP cells were recruited under our experimental conditions. We also observed two TML cells, which had the soma located at the border between the GCL and hilus and axonal arborization across the entire ML, was recruited by PP stimulation with an input strength of more than 0.7 ($n = 2/4$; Fig. 12J). Taken together, these results suggest that the dynamic range of the GC population is primarily regulated by somatic INs, MOPP cells, and NGFCs.

Specific Types of INs Regulate I-O Transformations of the GC Population

PV⁺ INs, mainly BCs and AACs (chandelier cells), constitute soma-targeting INs (Ribak et al. 1990; Soriano et al. 1990), whereas SST⁺ INs, mainly HIPP cells, are a major subpopulation of dendrite-targeting INs in the DG (Savanthrapadian et al. 2014). To assess the influence of inhibition on the dynamic range of the GC population, we drove conditional expression of halorhodopsin-3.0 (eNpHR3.0) in glutamic acid decarboxylase-expressing (GAD65⁺) INs, PV⁺ INs, and SST⁺ INs. To achieve this, we bilaterally injected a recombinant adeno-associated virus serotype 5 (AAV5) encoding Cre-dependent eNpHR3.0-eYFP [AAV5:(*eNpHR-eYFP*)^{Cre}] into the ventral DG of *Gad65*⁻, *Pvalb*⁻, and *Sst-cre* mice (Fig. 13A). Six weeks after virus injection, hippocampal slices were obtained from those mice for electrophysiological recordings (Fig. 14-19). Fig. 13B shows that eYFP signals in the DG from *Gad65*⁻, *Pvalb*⁻, and *Sst-cre* mice revealed distinct expression patterns. Consistent with the presence of Cre expression in all GAD65⁺ neurons, eYFP signals were detected across all laminated areas in the DG (Fig. 13B left). By contrast, eYFP signals in the DG were separated and complementary in *Pvalb*⁻ and *Sst-cre* mice. Strong eYFP signals in slices from *Pvalb-cre* mice were exclusively detected in the GCL (Fig. 13B middle); whereas intense eYFP signals in the outer-third and middle-third of the ML and the hilus were observed in slices from *Sst-cre* mice (Fig. 13B right). Whole-cell recordings from eYFP⁺ neurons showed that delivery of amber light selectively silenced eYFP⁺ INs evoked either by current injection or by PP stimulation at ten-fold of threshold input strength through the activation of Cl⁻ influx pumps (Fig. 14).

To assess the influence of specific INs on GC population activities, we examined the evoked pSpikes in the DG evoked by single-shock PP stimulation (0.033 Hz; Fig. 15). Although silencing of either GAD65⁺ or PV⁺ INs greatly increased the pSpike at various stimulus intensities (Fig. 15B, C), the extent of the effect was different. The effect of silencing GAD65⁺ INs (maximal effect, 233 ± 33 % of control, n = 10; p < 0.01; Fig. 15B) was approximately 1.34-fold greater than that of silencing PV⁺ INs (maximal effect, 175 ± 22 % of control, n = 6; p < 0.05; Fig. 15C). In contrast, silencing SST⁺ INs had no effect on the pSpike evoked by single-shock PP stimulation at any given intensity (maximal effect, 105 ± 3 % of control, n = 5; p = 0.31; Fig. 15D). To verify that the lack of effect of silencing SST⁺ INs was not due to poor expression efficiency, we bilaterally injected [AAV5:(*eNpHR-eYFP*)^{Cre}] into the ventral DG of *Gad65*- and *Sst-cre/Ai14* mice. We found that although the expression efficiency of eNpHR-eYFP is similar in *Gad65*- and *Sst-cre/Ai14* mice (83 ± 1 % vs 83 ± 2 %; Fig. 16A, B, D), optogenetic silencing of SST⁺ INs still had no effect on the pSpike in the DG (Fig. 16E). These results indicated that PV⁺, but not SST⁺, INs, regulate GC I-O transformations in response to single-shock stimulation. Furthermore, the greater effect of silencing GAD65⁺ INs versus PV⁺ INs indicates that other types of INs such as MOPP cells and NGFCs are likely involved in the regulation of GC spike generation.

PV⁺ INs Constrain the Cortical Dynamic Range of the GC Population

We next investigated the effect of silencing genetically-defined INs on the dynamic range of the GC population. Similar to GABA_A receptor blockade, optogenetic silencing of GAD65⁺ INs caused a

dramatic increase in the spiking probability and a reduction in the threshold input strength ($p < 0.01$, $n = 10$; Fig. 17A). In addition to the reduction of the activation threshold of spiking GCs, silencing of GAD65⁺ INs also activated most non-spiking GCs (Fig. 17B; green dashed lines and pie chart; non-spiking (NS) percentage from 48% to 7%). The synergy of these two effects expanded the dynamic range of the GC population in response to single-shock stimulation (Fig. 17C). Similar to GAD65⁺ INs, optogenetic silencing of PV⁺ INs significantly increased the spiking probability and decreased the threshold input strength of individual GCs ($p < 0.01$, $n = 12$; Fig. 17D). It also activated some non-spiking (NS) GCs (Fig. 17E; pink dashed lines and pie chart; NS percentage from 60% to 40%), leading to an moderately enhanced dynamic range of the GC population in response to single-shock stimulation (Fig. 17F). Conversely, neither the threshold input strength of individual GCs ($p = 1$, $n = 20$; Fig. 17G) nor the percentage of spiking GCs (Fig. 16H) was affected by silencing of SST⁺ INs under the same conditions. As a result, optogenetic silencing of SST⁺ INs had minimal influence on the dynamic range of the GC population during sparse activities (Fig. 17I). Together, these results indicate that PV⁺, but not SST⁺, INs, act primarily to regulate the offset of GC I-O transformations, thereby greatly restricting the cortical dynamic range.

PV⁺ and SST⁺ INs Differentially Regulate GC Population Spikes in the Series

In the engaged hippocampal network, the DG exhibits θ (4–8 Hz) and γ (30–80 Hz) frequency oscillations, both of which depend mainly on excitatory inputs from the EC (Bragin et al. 1995; Penttonen et al. 1998; Igarashi et al. 2014). With cell type-specific targeting, we investigated the role

of various INs in the recruitment of the GC population by stimulating the PP at various frequencies. Here we delivered 10- and 30-Hz trains, which mimic θ and γ rhythm frequency inputs, respectively, from the EC, to the PP. We found that silencing of GAD65⁺ INs robustly enhanced all pSpikes during 10- and 30-Hz trains (-GAD65, green traces; 10 Hz, n = 9; 30 Hz, n = 11; Fig. 18A, B), whereas silencing of PV⁺ and SST⁺ INs differentially increased the pSpikes in the series (-PV, magenta trace; 10 Hz, n = 7; 30 Hz, n = 13; -SST, blue traces; 10 Hz, n = 5; 30 Hz, n = 13; Fig. 18A, B). Overall, silencing GAD65⁺ INs robustly enhanced the first two pSpikes to the same extent in response to 10- and 30-Hz trains. However, the effect of silencing GAD65⁺ INs on late pSpikes was frequency dependent. Silencing GAD65⁺ INs resulted in a greater increase in the late phase of spike series at 30 Hz than that at 10 Hz (Fig. 18A-C). Conversely, silencing PV⁺ INs had greater effects on late spike series at 10 Hz than that at 30 Hz (Fig. 18A, B, D). Furthermore, silencing SST⁺ INs had similar effects on pSpikes in the late spike series during 10- and 30-Hz trains (Fig. 18A, B, E). By the way, these results also revealed that, in a series of strong upstream inputs coming from cortex either in θ or γ rhythm frequency, the GC population was efficiently activated by the second inputs due to relatively low inhibition-to-excitation ratios (Fig. 18).

To further examine how these INs differentially modulate a series of spikes in the GCs, we made whole-cell current-clamp recordings to investigate the spiking probability of individual GCs. We found that silencing GAD65⁺ INs greatly increased the spiking probability of either spiking or non-spiking individual GCs during the entire series (-GAD65, n = 5; Fig. 19); whereas inactivation of PV⁺

and SST⁺ INs differentially increased the spiking probability of the onset and later phase in spike series, respectively (-PV, n = 8, -SST, n = 8; Fig. 19). These results suggested that various types of INs differentially regulate the recruitment of the GC population through controlling the spike probabilities of individual spiking and non-spiking GCs.



DISCUSSION

Summary

Spiking of GCs in the developing and adult hippocampus is primarily regulated by synaptic inhibition originating from local GABAergic INs within the DG. Here we demonstrate that regulation of GC I-O relationships by specific types of INs depends on the cortical input patterns. In addition to soma-targeting INs including BCs and AACs, two types of ML INs, namely, MOPP cells and NGFCs, contribute to feedforward inhibition in the GCs during PP activation and thus regulate GC spiking to single-shock stimulation to the PP. Furthermore, PV⁺ INs, which are soma-targeting INs, and SST⁺ INs, a major population of dendrite-targeting INs, differentially restrict GC spiking during θ - γ activities. In sum, different IN types in the DG coordinate to regulate cortical signal transformations during various activity patterns.

Comparison to Previous Studies

The DG uses sparse population coding, wherein only a small portion of GCs can be recruited by cortical excitatory inputs. The percentage (47%) of GCs recruited with the stimulating paradigm used in the present study is relatively higher than those in previous reports (approximately 21% in Dieni et al. 2013; approximately 20% in Yu et al. 2013). At least two possible reasons may account for this discrepancy: first, unlike previous reports, in which the stimulation electrodes were placed in the molecular layer for MPP or LPP stimulation, we placed the stimulation electrode in the subiculum instead of the ML to avoid the direct activation of IN axons, which may activate both MPP and LPP

simultaneously (Marín-Burgin et al. 2012; Dieni et al. 2013; Yu et al. 2013). Second, we sampled GC populations with relatively large pSpikes to calibrate the input strength. Therefore, we might have overestimated the ratio of recruited GCs in a population. In spite of the difference due to our experimental paradigm, our major finding on how different types of INs modulate the recruitment of GCs here is not influenced by this discrepancy.

In the previous study, the authors questioned the validity of applying the calibration method used in CA1 region by Pouille et al. (2009) to the DG since they found the fEPSP in DG did not increase linearly with stimulus intensity and only a fraction of GCs could be activated regardless of stimulus intensity (Dieni et al. 2013). Furthermore, another study showed that the GCs in the suprapyramidal and infrapyramidal blades of DG may receive different levels of GABAergic inhibition, which dominantly regulate the spiking probabilities of local GCs (Yu et al. 2013). As a result, here we performed a control experiment to confirm that the calibration method is suitable for the DG GC population. We placed the stimulus electrodes in the subiculum and recorded the fEPSP and pSpike in three different regions of DG, suprapyramidal blade, infrapyramidal blade, and somewhere between them, in the same slice and stimulated at various stimulus intensities to establish the local input-output curves and do the calibration (Fig. 20). We found that after the calibration, the activation curves of local GC population almost overlap each other, which means the calibration at least expunged the difference within the same slice.

Our main finding is strikingly different to that of a recent study of the CA1 region (Lovett-Barron et al. 2012), where dendritic inhibition primarily restricts PC firing. Using a pharmacogenetic approach, Lovett-Barron et al. (2012) found that silencing SST⁺ dendrite-targeting INs, but not PV⁺ soma-targeting INs, increases the firing rate of CA1 PCs in response to SC input. Their result is unexpected in light of the widely held-belief that soma-targeting inhibitory INs control the spike initiation of principal neurons via axonal innervations onto perisomatic areas of principal neurons (Cobb et al. 1995; Miles et al. 1996; Kraushaar and Jonas 2000). Furthermore, they found that PV⁺ INs primarily inhibit a subtype of SST⁺ INs named ‘bistratified INs’, which target the proximal dendrites of CA1 PCs during CA3 SC input. The disinhibition of SST⁺ bistratified INs can compensate for a withdrawal of perisomatic inhibition. With the existence of proposed reciprocal connections between SST⁺ INs and PV⁺ INs in the CA1 region, silencing SST⁺ INs, in contrast, releases dendritic NMDA receptor-initiated electrogenesis, which cannot be overcome by disinhibition of PV⁺ INs, leading to increased firing of PCs. Unlike CA1 PCs, GCs use distinct dendritic mechanisms for input processing. First, GC dendrites act as a strong voltage attenuator, which strongly attenuates synaptic inputs along dendrites (Schmidt-Hieber et al. 2007; Krueppel et al. 2011). Second, GC dendrites are linear, meaning that they summate synaptic inputs linearly and are not designed for highly efficient synchrony detection (Krueppel et al. 2011). Third, GC dendrites lack dendritic spikes that would allow them to be more efficiently to bring EPSPs to AP threshold (Krueppel et al. 2011). Furthermore, SST⁺ INs in the DG all target to the distal dendrites of GCs, so

that disinhibition of SST⁺ INs, if there is any, may not compensate for a reduction of perisomatic inhibition. Taken together, distinct inhibitory microcircuits between the DG and CA1 regions, and passive properties of dendrites in GCs (Krueppel et al. 2011) likely account for this difference.

The Definition of “Dynamic Range”

In this study and previous one done by Pouille and his colleagues, the dynamic range is defined as the ratio of the input strengths that activate 95% versus 5% of the neuronal population. Since the ‘dynamic range’ means the range that ‘whole population’ can respond, the best way is to calculate the ratio of 100% to 0% recruitment. However, it’s quite difficult to estimate the input strength at 100% and 0% recruitment since the variation increases dramatically when it includes the extreme cases or you will never know whether all the population is activated or not. As a result, we choose to exclude 5% of two tails of population as error and preserve 90% of population to do further examination. Since we cumulatively plot the threshold input strength of single cells to make population activation curves, the dynamic range of single cells will not affect the dynamic range of whole population. Although fig. 4A, B shows that the dynamic range of single cells exhibit no difference between GC and CA1PC population, it is not inconsistent with the conclusion the GC population shows narrower dynamic range than CA1PC population. The similar phenomena is also observed in the change of dynamic range of individual GCs and GC population after gabazine application (Fig. 11).

Shunting Inhibition Offsets GC I-O Relationships and Reduces Gain during Synaptic Excitation

Individual PCs in the CA1 area display a wide range of sensitivity to input stimuli, allowing the population as a whole to represent a wider input range (Pouille et al. 2009). Feedforward inhibition, acting homogeneously across the PCs, rapidly adjusts their excitability to the strength of incoming afferent activity. As a result, the EP_{SGT} is dynamic and increases with the strength of the input (Pouille et al. 2009). A previous computational study also suggests that a dynamic EP_{SGT} is essential for the neuronal population to respond to a wide range of inputs. Such a dynamic EP_{SGT} is also observed in somatosensory cortex (Pouille et al. 2009). In contrast to CA1 PCs, the EP_{SGT} of individual GCs in the population is fixed and related to the input resistance of individual GCs but independent of threshold input strengths. Furthermore, mature, but not young, GCs have a high activation threshold due to low input resistance and strong GABAergic inhibition (Marín-Burgin et al. 2012). A higher threshold input strength accounts for the shift of activation curve to the right. Notably, the gain of individual GCs is much smaller than that of individual CA1 PCs recruited at weak input strength, thereby allowing each neuron in the population to respond over a wider range of input strengths. Therefore, unlike the CA1 PC model with a fixed EP_{SGT} (Pouille et al. 2009), the population activation curve of the GCs is only slightly steeper than that of CA1 PC population. Taken together, shunting inhibition in the DG has a dual effect: it offsets GC I-O relationships and reduces neuronal gain during synaptic excitation (Mitchell and Silver 2003).

A Lack of Synaptic Input Normalization in the GC Population

In striking contrast to the CA1 PC population, the amplitude of the EPSC needed to fire GCs is independent of the total number of active afferents. In other words, there is no synaptic input normalization for the GC population. What accounts for a fixed $EPSC_T$? Compared with CA1 INs, soma-targeting INs and ML INs in the DG are more easily recruited by small input strengths. As a result, the number of these recruited INs may not increase with stimulus strength, thereby resulting in a fixed $IPSC_T$ over the range of input strengths. Since feedforward inhibition does not increase in proportion to the input strength, it cannot dynamically adjust the activation threshold for GCs to reach spike threshold. Therefore, the $EPSC_T$ does not vary with the strength of the input.

We know that the intrinsic properties of GCs do not correlate with threshold input strengths (Fig. 5 and Fig. 21 for rats and mice, respectively). Why do GCs display variable threshold input strengths? We found that the $EPSC_T$, but not $IPSC_T$, negatively correlates with the input resistance (Fig. 22). This is consistent with the notion that the GCs with similar resting membrane potentials but with lower input resistance require more excitatory currents to reach AP threshold. Interestingly, given that the input resistance of GCs does not change with the threshold input strength (Fig. 5), it suggests that GCs with lower input resistance may receive more profuse excitatory afferent innervation.

Another intriguing question is: what are the distinct properties that determine GCs spiking? A small proportion of non-spiking GCs transformed into spiking cells after pharmacological of $GABA_A$

receptor blockade. A detailed analysis of intrinsic properties, excitatory and inhibitory synaptic drives of these cells ('NS→S cell') revealed that they have a higher AP threshold and a higher I/E ratio than spiking GCs, suggesting that the I/E ratio is an important factor in setting the activation threshold of GCs (Fig. 23).

Bidirectional Regulation of Spike Timing by GABAergic Conductance in the DG GCs

Previous studies indicated that both phasic and tonic GABAergic inhibition can regulate the spike timing of principal neurons in different ways (Pouille and Scanziani 2001; Kwag and Paulsen 2009; Wlodarczyk et al. 2013). The GC activities are tightly controlled by GABAergic inhibition in the DG, which includes tonic and phasic inhibition, thus the spike timing of individual GCs triggered by cortical inputs may also be deeply affected by GABAergic conductance. After we analyzed the spike latency of GCs before and after the gabazine treatment, we found that reducing inhibition could shorten the spike latency and jitter when input strength remains the same as threshold input strength measured in control condition. However, when input strength was decreased to the threshold under gabazine application, the spike latency and jitter of GCs become increase compared to the control condition. (Fig. 24).

Frequency-Tuned Distribution of Inhibition

The complete removal of inhibition from the DG following silencing of GAD67⁺ INs results in an increase in pSpikes with variable degrees at different timing during θ - γ activity, reflecting frequency-

tuned distribution of inhibition in the DG. Indeed, our recent study (Liu et al. 2014) shows that fast-spiking INs, which are soma-targeting INs, and non-fast-spiking INs, which are dendrite-targeting INs (consisting of HICAP and HIPP cells), are differentially recruited by excitatory inputs and in turn provide exquisite spatiotemporal control over GC activity. Using paired recordings from INs and GCs, we show that inhibition in the DG is dominated by somatic GABAergic inputs during periods of sparse (0.2 Hz) presynaptic activity; whereas dendritic GABAergic inputs are rapidly shifted to powerful and sustained inhibition during periods of intense (30–90 Hz) presynaptic activity (Liu et al. 2014). Consistent with our previous findings, the change of GC population response following silencing of SST⁺ INs is minimal to single-pulse stimulation of the PP (Fig. 15D). Furthermore, the delayed recruitment of dendrite-targeting INs and enhanced dendritic inhibition during γ activity can also account for marked increases in the late pSpikes following the complete removal of inhibition by silencing GAD65⁺ INs (Fig. 18B, E). Notably, such frequency-tuned inhibition is cell type-dependent and input pattern-dependent. Suppression mediated by PV⁺ INs at near- θ rhythm frequency is greater than that at γ -frequency (Fig. 18D). This is attributed to more reliable recruitment of PV⁺ INs and less depression of PV⁺ IN output synapses at 10 Hz compared with 30 Hz (Kraushaar and Jonas 2000; Ewell and Jones 2010). In contrast to PV⁺ INs, no difference in SST⁺ IN-mediated suppression is observed between 10 and 30 Hz.

The increase in pSpikes following silencing of GAD65⁺ INs (approximately 2.4-fold) is similar to that following GABA_AR blockade with gabazine (approximately 2.7-fold; Fig. 25), but is almost

2-fold greater than that following silencing of PV⁺ INs (Fig. 15). Various types of INs are identified in the DG (Freund and Buzsáki 1996; Hosp et al. 2014; Liu et al. 2014). In our experiments, HICAP and HIPP cells cannot be recruited by PP stimulation under the stimulating paradigm, suggesting that they are primarily targeted by the mossy fibers from GCs, commissural–associational (C/A) pathway from hilar mossy cells or other inputs and may serve as feedback inhibitors to GCs. Fig. 12 showed that MOPP cells and NGFCs are likely to participate in controlling the dynamic range of the GC population according to their threshold input strength and spike delay, but we did not have direct evidence to prove that these INs do affect GCs during PP stimulation. According to previous studies, both MOPP cells and NGFCs are considered as primary feedforward inhibitory interneurons in the DG (Armstrong et al. 2011; Li et al. 2013), and in this study we showed that probably half of the optogenetic silencing effects of GAD65⁺ INs originated from these ML INs (Fig. 15). Furthermore, an elegant study recently done in our lab performed that although ML INs could only be recruited in the initial phase of 10 Hz spike series by optogenetic activation of MPP, but these ML INs could instead be activated by C/A pathway during whole spike series (Hsu et al. 2015). These results indicated that ML INs not only serve as feedforward inhibitors but also play an important role in feedback inhibition in the DG. However, due to lack of specific biomarkers of MOPP cells and NGFCs, we could not specifically suppress these ML INs and studied their effects on I-O transformation of the GC population. Although both MOPP cells and NGFCs are likely to participate in controlling the dynamic range of the GC population, NGFCs may have a less effect than MOPP

cells on the onset of spike series due to their slower kinetics of synaptic release (Armstrong et al. 2011), but may generate long-lasting GABAergic currents and play an important role during repetitive PP activation.



REFERENCES

- Acsády L, Káli S. 2007. Models, structure, function: the transformation of cortical signals in the dentate gyrus. *Prog Brain Res.* 163:577-599.
- Adrian ED, Zotterman Y. 1926. The impulses produced by sensory nerve-endings. Part 2. The response of a single end-organ. *J Physiol.* 61:151–171.
- Adrian ED, Zotterman Y. 1926. The impulses produced by sensory nerve endings. Part 3. Impulses set up by touch and pressure. *J Physiol.* 61:465–483.
- Aimone JB, Deng W, Gage FH. 2011. Resolving new memories: a critical look at the dentate gyrus, adult neurogenesis, and pattern separation. *Neuron.* 70(4):589-596.
- Alger BE, Nicoll RA. 1979. GABA-mediated biphasic inhibitory responses in hippocampus. *Nature.* 281:315-317.
- Alme CB, Buzzetti RA, Marrone DG, Leutgeb JK, Chawla MK, Schaner MJ, Bohanick JD, Khoboko T, Leutgeb S, Moser EI, Moser MB, McNaughton BL, Barnes CA. 2010. Hippocampal granule cells opt for early retirement. *Hippocampus.* 20:1109-1123.
- Altman J, Das GD. 1965. Autoradiographic and histological evidence of postnatal neurogenesis in rats. *J Comp Neurol.* 124:319-335.
- Amaral DG, Lavenex P. 2006. "Ch 3. Hippocampal Neuroanatomy". In Andersen P, Morris R, Amaral DG, Bliss T, O'Keefe J. *The Hippocampus Book.* Oxford University Press.
- Amaral DG, Scharfman HE, Lavenex P. 2007. The dentate gyrus: fundamental neuroanatomical organization (dentate gyrus for dummies). *Prog Brain Res.* 163:3–22.
- Andersen P, Bliss TV, Skrede KK. 1971. Lamellar organization of hippocampal excitatory pathways. *Exp Brain Res.* 13:222–238.
- Andersen P. 1975. Organization of hippocampal neurons and their interconnections. In Isaacson RL, Pribram KH. *The Hippocampus.* 155-175.
- Andersen P, Dingledine R, Gjerstad L, Langmoen IA, Laursen AM. 1980. Two different responses of hippocampal pyramidal cells to application of gamma-amino butyric acid. *J Physiol.* 305:279-296.
- Armstrong C, Szabadics J, Tamás G, Soltesz I. 2011. Neurogliaform cells in the molecular layer of

the dentate gyrus as feed-forward γ -aminobutyric acidergic modulators of entorhinal-hippocampal interplay. *J Comp Neurol*. 519:1476-1491.

Bakker A, Kirwan CB, Miller M, Stark CE. 2008. Pattern separation in the human hippocampal CA3 and dentate gyrus. *Science*. 319(5870):1640-1642.

Bartos M, Vida I, Frotscher M, Meyer A, Monyer H, Geiger JR, Jonas P. 2002. Fast synaptic inhibition promotes synchronized gamma oscillations in hippocampal interneuron networks. *Proc Natl Acad Sci USA*. 99:13222-13227.

Bartos M, Vida I, Jonas P. 2007. Synaptic mechanisms of synchronized gamma oscillations in inhibitory interneuron networks. *Nat Rev Neurosci*. 8(1):45-56.

Bliss TV, Lomo T. 1973. Long-lasting potentiation of synaptic transmission in the dentate area of the anaesthetized rabbit following stimulation of the perforant path. *J Physiol*. 232(2):331-356.

Boyett JM, Buckmaster PS. 2001. Somatostatin-immunoreactive interneurons contribute to lateral inhibitory circuits in the dentate gyrus of control and epileptic rats. *Hippocampus*. 11:418-422.

Brady DR, Mufson EJ. 1997. Parvalbumin-immunoreactive neurons in the hippocampal formation of Alzheimer's diseased brain. *Neuroscience*. 80(4):1113-1125.

Bragin A, Jandó G, Nadásdy Z, Hetke J, Wise K, Buzsáki G. 1995. Gamma (40-100 Hz) oscillation in the hippocampus of the behaving rat. *J Neurosci*. 15:47-60.

Brickley SG, Cull-candy SG, Farrant M. 1996. Development of a tonic form of synaptic inhibition in rat cerebellar granule cells resulting from persistent activation of GABAA receptors. *J Physiol (Lond)*. 497: 753-759.

Broglio C, Gómez A, Durán E, Ocaña FM, Jiménez-Moya F, Rodríguez F, Salas C. 2005. Hallmarks of a common forebrain vertebrate plan: specialized pallial areas for spatial, temporal and emotional memory in actinopterygian fish. *Brain Res Bull*. 66 (4-6):397-399.

Buzsaki G. 2010. Neural syntax: cell assemblies, synapsembles, and readers. *Neuron*. 68:362-385.

Cajal SR. 1893. Estructura del asta de Ammon. *Anal Soc Esp Hist Nat*. Madrid 22:53-114.

Cajal SR. 1933. *Histology*, 10th ed. Baltimore: Wood.

- Carvalho TP, Buonomano DV. 2009. Differential effects of excitatory and inhibitory plasticity on synaptically driven neuronal input-output functions. *Neuron*. 61:774-785.
- Cash S, Yuste R. 1999. Linear summation of excitatory inputs by CA1 pyramidal neurons. *Neuron*. 22(2):383-94.
- Chance FS, Abbott LF, Reyes AD. 2002. Gain modulation from background synaptic input. *Neuron*. 35:773-782.
- Chawla MK, Guzowski JF, Ramirez-Amaya V, Lipa P, Hoffman KL, Marriott LK, Worley PF, McNaughton BL, Barnes CA. 2005. Sparse, environmentally selective expression of Arc RNA in the upper blade of the rodent fascia dentata by brief spatial experience. *Hippocampus*. 15:579-586.
- Chiang PH, Wu PY, Kuo TW, Liu YC, Chan CF, Chien TC, Cheng JK, Huang YY, Chiu CD, Lien CC. 2012. GABA is depolarizing in hippocampal dentate granule cells of the adolescent and adult rats. *J Neurosci*. 32(1):62-67.
- Chklovskii DB. 2004. Synaptic connectivity and neuronal morphology: two sides of the same coin. *Neuron*. 43:609-617.
- Cobb SR, Buhl EH, Halasy K, Paulsen O, Somogyi P. 1995. Synchronization of neuronal activity in hippocampus by individual GABAergic interneurons. *Nature*. 378:75-78.
- Colombo M, Broadbent N. 2000. Is the avian hippocampus a functional homologue of the mammalian hippocampus? *Neurosci Biobehav Rev* 24(4):465-484.
- Coulter DA, Carlson GC. 2007. Functional regulation of the dentate gyrus by GABA-mediated inhibition. *Prog Brain Res*. 163:235-243.
- Csicsvari J, Jamieson B, Wise KD, Buzsáki G. 2003. Mechanisms of gamma oscillations in the hippocampus of the behaving rat. *Neuron*. 37(2):311-322.
- Curtis DR, Watkins JC. 1960. The excitation and depression of spinal neurones by structurally related amino acids. *J Neurochem*. 6:117-141.
- Dancause N, Barbay S, Frost SB, Plautz EJ, Popescu M, Dixon PM, Stowe AM, Friel KM, Nudo RJ. 2005. Topographically divergent and convergent connectivity between premotor and primary motor cortex. *Cereb Cortex*. 16:1057-1068.

Deng W, Aimone JB, Gage FH. 2010. New neurons and new memories: how does adult hippocampal neurogenesis affect learning and memory? *Nature Rev Neurosci.* 11:339–350.

Denny CA, Burghardt NS, Schachter DM, Hen R, Drew MR. 2012. 4- to 6-week-old adult-born hippocampal neurons influence novelty-evoked exploration and contextual fear conditioning. *Hippocampus.* 22:1188–1201.

Dieni CV, Nietz AK, Panichi R, Wadiche JI, Wadiche LO. 2013. Distinct determinants of sparse activation during granule cell maturation. *J Neurosci.* 33:19131-19142.

Diesmann M, Gewaltig MO, Aertsen A. 1999. Stable propagation of synchronous spiking in cortical neural networks. *Nature.* 402:529-533.

Doiron B, Longtin A, Berman N, Maler L. 2001. Subtractive and divisive inhibition: effect of voltage-dependent inhibitory conductances and noise. *Neural Comput.* 13:227–248.

Dupret D, Pleydell-Bouverie B, Csicsvari J. 2008. Inhibitory interneurons and network oscillations. *Proc Natl Acad Sci U S A.* 105(47):18079-18080.

Eichenbaum H, Otto TA, Wible CG, Piper JM. 1991. Ch 7. Building a model of the hippocampus in olfaction and memory. In Davis JL, Eichenbaum H. *Olfaction.* MIT Press.

Eriksson PS, Perfilieva E, Björk-Eriksson T, Alborn AM, Nordborg C, Peterson DA, Gage FH. 1998. Neurogenesis in the adult human hippocampus. *Nat Med.* 4:1313–1317.

Ewell LA, Jones MV. 2010. Frequency-tuned distribution of inhibition in the dentate gyrus. *J Neurosci.* 30:12597-12607.

Farrant M, Nusser Z. 2005. Variations on an inhibitory theme: phasic and tonic activation of GABA(A) receptors. *Nat Rev Neurosci.* 6(3):215-229.

Fell J, Klaver P, Lehnertz K, Grunwald T, Schaller C, Elger CE, Fernández G. 2001. Human memory formation is accompanied by rhinal-hippocampal coupling and decoupling. *Nat Neurosci.* 4(12):1259-1264.

Földy C, Lee SY, Szabadics J, Neu A, Soltesz I. 2007. Cell type-specific gating of perisomatic inhibition by cholecystinin. *Nat Neurosci.* 10(9):1128-1130.

- Freund TF, Buzsáki G. 1996. Interneurons of the hippocampus. *Hippocampus*. 6:347-470.
- Geiger JR, Lübke J, Roth A, Frotscher M, Jonas P. 1997. Submillisecond AMPA receptor-mediated signaling at a principal neuron-interneuron synapse. *Neuron*. 18(6):1009-1023.
- Georgopoulos AP, Schwartz AB, Kettner RE. 1986. Neuronal population coding of movement direction. *Science*. 233(4771):1416-1419.
- Golding NL, Spruston N. 1998. Dendritic sodium spikes are variable triggers of axonal action potentials in hippocampal CA1 pyramidal neurons. *Neuron*. 21:1189–1200.
- Gu Y, Arruda-Carvalho M, Wang J, Janoschka SR, Josselyn SA, Frankland PW, Ge S. 2012. Optical controlling reveals time-dependent roles for adult-born dentate granule cells. *Nat Neurosci* 15:1700–1706.
- Hájos N, Acsády L, Freund TF. 1996. Target selectivity and neurochemical characteristics of VIP-immunoreactive interneurons in the rat dentate gyrus. *Eur J Neurosci*. 8:1415-1431.
- Halasy K, Somogyi P. 1993. Subdivisions in the multiple GABAergic innervation of granule cells in the dentate gyrus of the rat hippocampus. *Eur J Neurosci*. 5:411–429.
- Hoffman DA, Magee JC, Colbert CM, Johnston D. 1997. K⁺ channel regulation of signal propagation in dendrites of hippocampal pyramidal neurons. *Nature*. 387:869–875.
- Hofman MA. 2014. Evolution of the human brain: when bigger is better. *Front Neuroanat*. 8:15.
- Hosp JA, Strüber M, Yanagawa Y, Obata K, Vida I., Jonas P, Bartos M. 2014. Morpho-physiological criteria divide dentate gyrus interneurons into classes. *Hippocampus*. 24:189–203.
- Hu T, Towfic ZJ, Pehlevan C, Genkin A, Chklovskii DB. 2014. A Neuron as a Signal Processing Device. *IEEE*. 362-366.
- Hsu TT, Lee CT, Tai MH, Lien CC. 2015. Differential Recruitment of Dentate Gyrus Interneuron Types by Commissural Versus Perforant Pathways. *Cereb Cortex*. Published online.
- Igarashi KM, Lu L, Colgin LL, Moser MB, Moser EI. 2014. Coordination of entorhinal-hippocampal ensemble activity during associative learning. *Nature*. 510:143-147.

- Jacobs LF. 2003. The evolution of the cognitive map. *Brain Behav Evol.* 62(2):128–139.
- Jonas P, Buzsaki G. 2007. Neural inhibition. *Scholarpedia.* 2(9):3286.
- Kampa BM, Stuart GJ. 2006. Calcium spikes in basal dendrites of layer 5 pyramidal neurons during action potential bursts. *J Neurosci.* 26(28):7424-7432.
- Kesner RP. 2013. An analysis of the dentate gyrus function. *Behav Brain Res.* 254:1-7.
- Kraushaar U, Jonas P. 2000. Efficacy and stability of quantal GABA release at a hippocampal interneuron-principal neuron synapse. *J Neurosci.* 20:5594-5607.
- Krnjevic K, Schwartz S. 1967. The action of γ -aminobutyric acid on cortical neurones. *Exp. Brain Res.* 3:320–326.
- Krueppel R, Remy S, Beck H. 2011. Dendritic integration in hippocampal dentate granule cells. *Neuron.* 71:512-528.
- Kullmann DM. 2011. Interneuron networks in the hippocampus. *Curr Opin Neurobiol.* 21:709-716.
- Kwag J, Paulsen O. 2009. Bidirectional control of spike timing by GABA(A) receptor-mediated inhibition during theta oscillation in CA1 pyramidal neurons. *Neuroreport.* 20(13):1209-1213.
- Larimer P, Strowbridge BW. 2010. Representing information in cell assemblies: persistent activity mediated by semilunar granule cells. *Nat Neurosci.* 13(2):213-222.
- Leutgeb JK, Leutgeb S, Moser MB, Moser EI. 2007. Pattern separation in the dentate gyrus and CA3 of the hippocampus. *Science.* 315:961-966.
- Li Y, Stam FJ, Aimone JB, Goulding M, Callaway EM, Gage FH. 2013. Molecular layer perforant path-associated cells contribute to feed-forward inhibition in the adult dentate gyrus. *Proc Natl Acad Sci USA.* 110:9106-9111.
- Liu YC, Cheng JK, Lien CC. 2014. Rapid dynamic changes of dendritic inhibition in the dentate gyrus by presynaptic activity patterns. *J Neurosci.* 34:1344-1357.
- Losonczy A, Magee JC. 2006. Integrative properties of radial oblique dendrites in hippocampal CA1 pyramidal neurons. *Neuron.* 50:291–307.

- Lovett-Barron M, Turi GF, Kaifosh P, Lee PH, Bolze F, Sun XH, Nicoud JF, Zemelman BV, Sternson SM, Losonczy A. 2012. Regulation of neuronal input transformations by tunable dendritic inhibition. *Nat Neurosci.* 15:423-430.
- Marín-Burgin A, Mongiat LA, Pardi MB, Schinder AF. 2012. Unique processing during a period of high excitation/inhibition balance in adult-born neurons. *Science.* 335:1238-1242.
- Marr D. 1969. A theory of cerebellar cortex. *J Physiol.* 202:437-470.
- McCulloch WS, Pitts W. 1943. A logical calculus of the ideas immanent in nervous activity. *Bull Math Biophys.* 5:115–133.
- Miles R, Tóth K, Gulyás AI, Hájos N, Freund TF. 1996. Differences between somatic and dendritic inhibition in the hippocampus. *Neuron.* 16:815-823.
- Mitchell SJ, Silver RA. 2003. Shunting inhibition modulates neuronal gain during synaptic excitation. *Neuron.* 38:433–445.
- Moodley KK, Chan D. 2014. The hippocampus in neurodegenerative disease. *Front Neurol Neurosci.* 34:95-108.
- Moser E, Moser MB, Andersen P. 1993. Spatial learning impairment parallels the magnitude of dorsal hippocampal lesions, but is hardly present following ventral lesions. *J Neurosci.* 13(9):3916-3925.
- Myatt DR, Hadlington T, Ascoli GA, Nasuto SJ. 2012. Neuromantic - from semi-manual to semi-automatic reconstruction of neuron morphology. *Front Neuroinform.* 6:4.
- Nadel L. 1968. Dorsal and ventral hippocampal lesions and behavior. *Physiol Behav.* 3:891–900.
- Nitz D, McNaughton B. 2004. Differential modulation of CA1 and dentate gyrus interneurons during exploration of novel environments. *J Neurophysiol.* 91:863–872.
- Nusser Z, Mody I. 2002. Selective modulation of tonic and phasic inhibitions in dentate gyrus granule cells. *J Neurophysiol.* 87(5):2624-2628.
- Olshausen BA, Field DJ. 2004. Sparse coding of sensory inputs. *Curr. Opin. Neurobiol.* 14:481–487.
- O'Keefe J, Dostrovsky J. 1971. The hippocampus as a spatial map. Preliminary evidence from unit

activity in the freely-moving rat. *Brain Res.* 34(1):171–175.

O'Keefe J, Nadel L. 1978. *The Hippocampus as a Cognitive Map*. Oxford University Press.

Otsuka J, Iversen LL, Hall ZW, Kravitz EA. 1966. Release of gamma-aminobutyric acid from inhibitory nerves of lobster. *Proc Natl Acad Sci USA.* 56:1110-1115.

Penttonen M, Kamondi A, Acsády L, Buzsáki G. 1998. Gamma frequency oscillation in the hippocampus of the rat: intracellular analysis in vivo. *Eur J Neurosci.* 10:718-728.

Portavella M, Vargas JP, Torres B, Salas C. 2002. The effects of telencephalic pallial lesions on spatial, temporal, and emotional learning in goldfish. *Brain Res Bull.* 57(3-4):397–399.

Pöschel B, Draguhn A, Heinemann U. 2002. Glutamate-induced gamma oscillations in the dentate gyrus of rat hippocampal slices. *Brain Res.* 938(1-2):22-28.

Pouille F, Marín-Burgin A, Adesnik H, Atallah BV, Scanziani M. 2009. Input normalization by global feedforward inhibition expands cortical dynamic range. *Nat Neurosci.* 12:1577-1585.

Pouille F, Scanziani M. 2001. Enforcement of temporal fidelity in pyramidal cells by somatic feed-forward inhibition. *Science.* 293:1159–1163.

Ramaswamy S. 2015. Exciting times for inhibition: GABAergic synaptic transmission in dentate gyrus interneuron networks. *Front Neural Circuits.* 9:13.

Ransome MI, Renoir T, Hannan AJ. 2012. Hippocampal neurogenesis, cognitive deficits and affective disorder in Huntington's disease. *Neural Plast.* 2012:874387.

Ribak CE, Nitsch R, Seress L. 1990. Proportion of parvalbumin-positive basket cells in the GABAergic innervation of pyramidal and granule cells of the rat hippocampal formation. *J Comp Neurol.* 300:449-461.

Ribak CE. 1992. Local circuitry of GABAergic basket cells in the dentate gyrus. *Epilepsy Res Suppl.* 7:29-47.

Rodríguez F, López JC, Vargas JP, Broglio C, Gómez Y, Salas C. 2002. Spatial memory and hippocampal pallium through vertebrate evolution: insights from reptiles and teleost fish. *Brain Res Bull.* 57(3-4):499–503.

- Rothman JS, Cathala L, Steuber V, Silver RA. 2009. Synaptic depression enables neuronal gain control. *Nature*. 457:1015–1018.
- Sahay A, Scobie KN, Hill AS, O'Carroll CM, Kheirbek MA, Burghardt NS, Fenton AA, Dranovsky A, Hen R. 2011. Increasing adult hippocampal neurogenesis is sufficient to improve pattern separation. *Nature*. 472:466–470.
- Sakurai Y. 1999. How do cell assemblies encode information in the brain? *Neurosci Biobehav Rev*. 23:785–796.
- Sambandan S, Sauer JF, Vida I, Bartos M. 2010. Associative plasticity at excitatory synapses facilitates recruitment of fast-spiking interneurons in the dentate gyrus. *J Neurosci*. 30:11826–11837.
- Savanthrapadian S, Meyer T, Elgueta C, Booker SA, Vida I, Bartos M. 2014. Synaptic properties of SOM- and CCK-expressing cells in dentate gyrus interneuron networks. *J Neurosci*. 34:8197-8209.
- Schmidt-Hieber C, Jonas P, Bischofberger J. 2004. Enhanced synaptic plasticity in newly generated granule cells of the adult hippocampus. *Nature*. 429(6988):184-187.
- Schmidt-Hieber C, Jonas P, Bischofberger J. 2007. Subthreshold dendritic signal processing and coincidence detection in dentate gyrus granule cells. *J Neurosci*. 27:8430-8441.
- Scoville WB, Milner B. 1957. Loss of recent memory after bilateral hippocampal lesions. *J Neurol Neurosurg Psychiatry*. 20(1):11–21.
- Semyanov A, Walker MC, Kullmann DM. 2003. GABA uptake regulates cortical excitability via cell type-specific tonic inhibition. *Nat Neurosci*. 6(5):484-490.
- Shadlen MN, Newsome WT. 1998. The variable discharge of cortical neurons: implications for connectivity, computation and information coding. *J Neurosci*. 18:3870-3896.
- Shu Y, Hasenstaub A, Badoual M, Bal T, McCormick DA. 2003. Barrages of synaptic activity control the gain and sensitivity of cortical neurons. *J Neurosci*. 23:10388-10401.
- Silver RA. Neuronal arithmetic. 2010. *Nat Rev Neurosci*. 11(7):474-489.
- Sloviter RS. 1991. Permanently altered hippocampal structure, excitability, and inhibition after experimental status epilepticus in the rat: the dormant basket cell hypothesis and its possible relevance

to temporal lobe epilepsy. *Hippocampus*. 1:41–66.

Sloviter RS, Zappone CA, Harvey BD, Bumanglag AV, Bender RA, Frotscher M. 2003. “Dormant basket cell” hypothesis revisited; relative vulnerabilities of dentate gyrus mossy cells and inhibitory interneurons after hippocampal status epilepticus in the rat. *J Comp Neurol*. 459:44–76.

Somogyi P, Tamas G, Lujan R, Buhl EH. 1998. Salient features of synaptic organisation in the cerebral cortex. *Brain Res Rev*. 26:113–135.

Soriano E, Nitsch R, Frotscher M. 1990. Axo-axonic chandelier cells in the rat fascia dentata: Golgi-electron microscopy and immunocytochemical studies. *J Comp Neurol*. 293:1-25.

Spalding KL, Bergmann O, Alkass K, Bernard S, Salehpour M, Huttner HB, Boström E, Westerlund I, Vial C, Buchholz BA, Possnert G, Mash DC, Druid H, Frisén J. 2013. Dynamics of hippocampal neurogenesis in adult humans. *Cell*. 153(6):1219-1227.

Staley KJ, Mody I. 1992. Shunting of excitatory input to dentate gyrus granule cells by a depolarizing GABA_A receptor-mediated postsynaptic conductance. *J Neurophysiol*. 68:197-212.

Stell BM, Mody I. 2002. Receptors with different affinities mediate phasic and tonic GABA(A) conductances in hippocampal neurons. *J Neurosci*. 22(10):RC223.

Strange BA, Witter MP, Lein ES, Moser EI. 2014. Functional organization of the hippocampal longitudinal axis. *Nat Rev Neurosci*. 15(10):655-669.

Tamamaki N, Nojyo Y. 1993. Projection of the entorhinal layer II neurons in the rat as revealed by intracellular pressure-injection of neurobiotin. *Hippocampus*. 3:471-480.

Tashiro A, Makino H, Gage FH. 2007. Experience-specific functional modification of the dentate gyrus through adult neurogenesis: a critical period during an immature stage. *J Neurosci*. 23:3252-3259.

Van Groen T, Wyss JM. 1990. Extrinsic projections from area CA1 of the rat hippocampus: olfactory, cortical, subcortical, and bilateral hippocampal formation projections. *J Comp Neurol*. 302(3):515-528.

van Groen T, Miettinen P, Kadish I. 2003. The entorhinal cortex of the mouse: organization of the projection to the hippocampal formation. *Hippocampus*. 13:133-149.

van Praag H, Schinder AF, Christie BR, Toni N, Palmer TD, Gage FH. 2002. Functional neurogenesis in the adult hippocampus. *415(6875):1030-1034.*

Varela F, Lachaux JP, Rodriguez E, Martinerie J. 2001. The brainweb: phase synchronization and large-scale integration. *Nat Rev Neurosci. 2(4):229–239.*

Vargas JP, Bingman VP, Portavella M, López JC. 2006. Telencephalon and geometric space in goldfish. *Eur J Neurosci. 24(10):2870–2878.*

Vinje WE, Gallant JL. 2000. Sparse coding and decorrelation in primary visual cortex during natural vision. *Science. 287:1273–1276.*

Vogels TP, Abbott LF. 2005. Signal propagation and logic gating in networks of integrate-and-fire neurons. *J Neurosci. 25:10786-10795.*

Werman R, Davidoff RA, Aprison MH. 1967. Inhibition of motoneurons by iontophoresis of glycine. *Nature. 214:681–683.*

West MJ. 1990. Stereological studies of the hippocampus: a comparison of the hippocampal subdivisions of diverse species including hedgehogs, laboratory rodents, wild mice and men. *Prog Brain Res. 83:13–36.*

Whittington MA, Traub RD. 2003. Interneuron diversity series: inhibitory interneurons and network oscillations in vitro. *Trends Neurosci. 26(12):676-682.*

Wlodarczyk AI, Xu C, Song I, Doronin M, Wu YW, Walker MC, Semyanov A. 2013. Tonic GABAA conductance decreases membrane time constant and increases EPSP-spike precision in hippocampal pyramidal neurons. *Front Neural Circuits. 7:205.*

Xue M, Atallah BV, Scanziani M. 2014. Equalizing excitation-inhibition ratios across visual cortical neurons. *Nature. 511(7511):596-600.*

Yu EP, Dengler CG, Frausto SF, Putt ME, Yue C, Takano H, Coulter DA. 2013. Protracted postnatal development of sparse, specific dentate granule cell activation in the mouse hippocampus. *J Neurosci. 33:2947-2960.*

Zheng K, Rusakov DA. 2015. Efficient Integration of Synaptic Events by NMDA Receptors in Three-Dimensional Neuropil. *Biophys J. 108(10):2457-2564.*

FIGURES AND TABLE

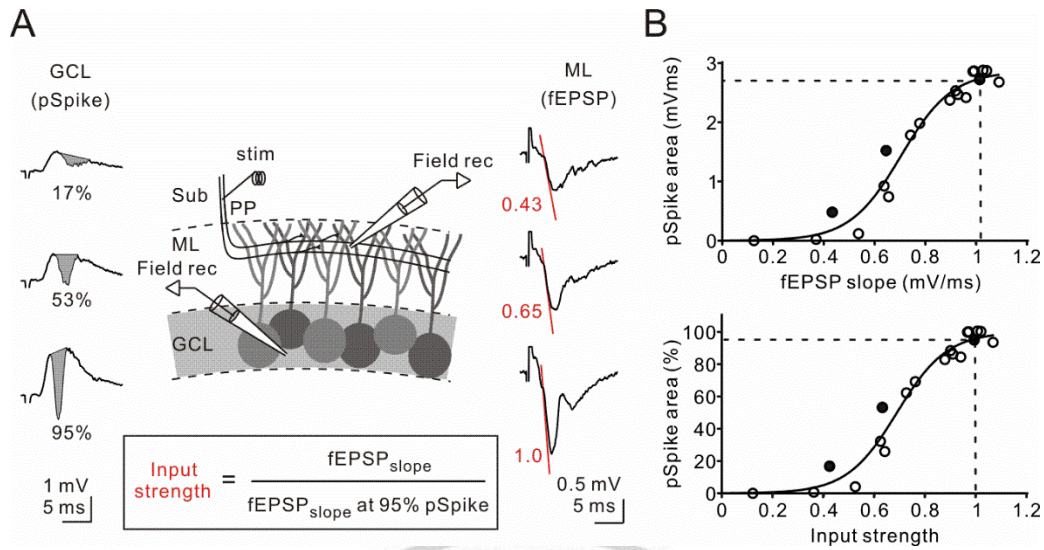


Fig. 1 Calibration of cortical input strength

(A) Schematic of recording configuration: a stimulation electrode (stim) was placed in the Sub to activate the PP fibers; two field recording electrodes (glass pipettes filled with ACSF) were placed in the GCL and in the ML to simultaneously detect the pSpike (left) and fEPSP (right), respectively, in response to single pulse delivered to the PP at varying stimulus strengths. The pSpike was calculated by the area (in gray). The input strength is the slope of the fEPSP ($\text{fEPSP}_{\text{slope}}$; red lines) elicited at any given stimulus intensity normalized to the $\text{fEPSP}_{\text{slope}}$ evoked at a stimulus intensity, which results in a pSpike of 95% of its maximal amplitude.

(B) Top, the pSpike area is plotted against fEPSP slope for the experiment illustrated in (A). Bottom, the normalized pSpike area is plotted against input strength for the same experiment. Data are fit with a sigmoid function. Filled symbols correspond to the example traces in (A).

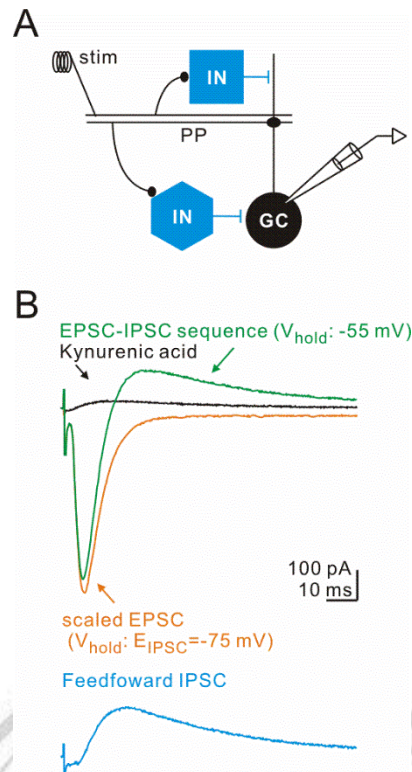


Fig. 2 Isolation of monosynaptic EPSCs and feedforward IPSCs

(A) Simplified diagram of feedforward inhibitory circuits and recording configuration. Stimulation of the PP evokes monosynaptic excitation and disynaptic inhibition via GABAergic INs onto GCs.

(B) Top traces, green trace: EPSC–IPSC sequence recorded in a GC V-clamped at -55 mV in response to PP stimulation. Orange trace: EPSC recorded at the reversal potential of the IPSC ($E_{IPSC} = -75$ mV) and scaled to the initial slope of the EPSC–IPSC sequence. Black trace: Recording at -55 mV in the presence of the ionotropic glutamate receptor antagonist kynurenic acid (2 mM), which abolishes the EPSC–IPSC sequence, indicating the disynaptic nature of the IPSC. Bottom trace, the feedforward IPSC (pale blue) was isolated by subtracting the scaled EPSC (orange) from the EPSC–IPSC sequence (green).

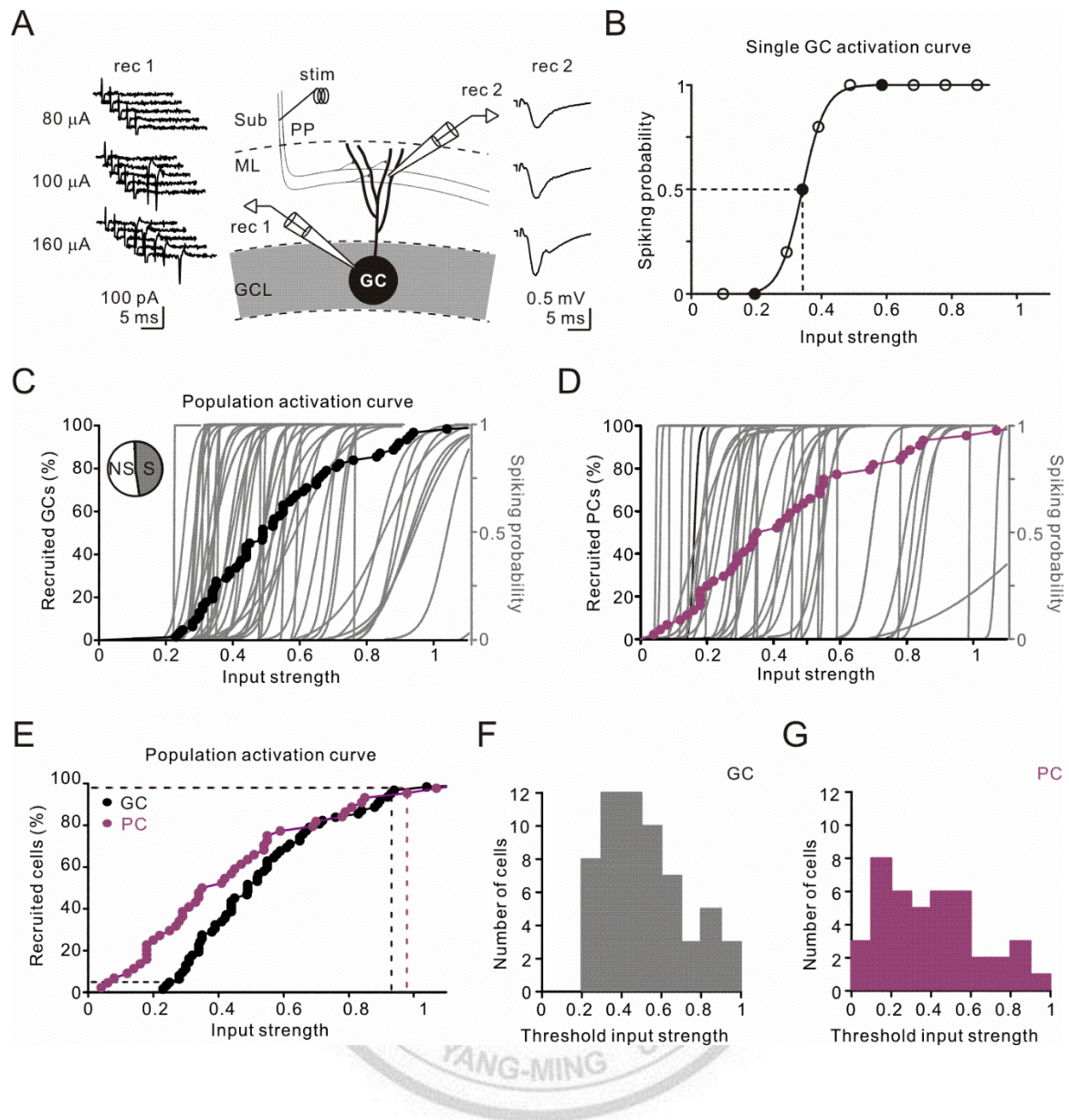


Fig. 3 The granule cell (GC) population shows narrow dynamic range

(A) Schematic of recording configuration: a stimulation electrode (stim) was placed in the subiculum (Sub) to activate the perforant path (PP); rec 1 represents loose-patch or cell-attached recording from a single GC; rec 2 represents field excitatory postsynaptic potential (fEPSP) recording in the molecular layer (ML). Example traces of action currents (left) recorded from a single GC in the cell-attached configuration and fEPSP recordings (right) in response to PP stimulation at increasing

stimulus intensities (80–160 μA , 100 μs). Stimulus artifacts are truncated for clarity.

(B) Spiking probability is plotted against input strength for a typical example of a GC (sigmoidal fit, dashed lines indicate the threshold input strength yielding 50% spiking probability). Filled symbols correspond to the example traces.

(C) Black points stand for the activation curve of the GC population (the cumulative plot of input strengths evoking 50% spiking probability, $n = 62/131$). Gray sigmoids indicate the activation curves of the 62 individual GCs as plotted in (B). The pie chart shows the percentage of spiking (S) and non-spiking (NS) GCs evoked by PP stimulation.

(D) Magenta points stand for the activation curve of the CA1 PC population (the cumulative plot of input strengths evoking 50% spiking probability, $n = 44/45$). Gray sigmoids indicate the activation curves of the 44 individual CA1 PCs.

(E) The cumulative activation curves of the spiking GC (black) and CA1 pyramidal cell (PC) (magenta) populations. Dashed lines indicate the input strengths recruiting 5% and 95% of each population.

(F) The histograms show the distribution of threshold input strengths of GCs.

(G) The distribution of threshold input strengths of CA1 PCs.

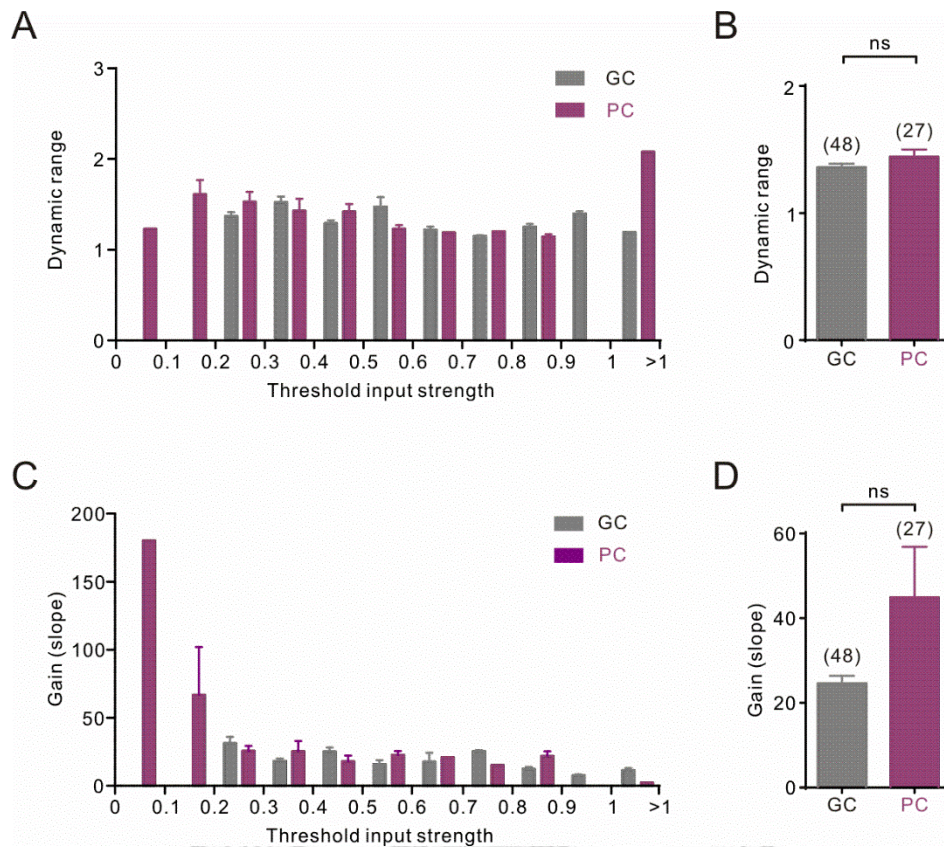


Fig. 4 The dynamic range and gain of individual cells are not significantly different between GC population and CA1 PC population

(A) The bar graph shows the dynamic range of individual GCs and PCs (i.e., the ratio of the input strengths triggering spikes in the cell in 95% versus 5% of the trials; GC in gray, PC in magenta) plotted against threshold input strength. Error bars indicate s.e.m..

(B) Summary plot of the dynamic range of individual GCs and PCs (GC in gray, PC in magenta). Error bars indicate s.e.m.; ns indicates nonsignificance, $p > 0.05$.

(C) The bar graph shows the gain of individual GCs and PCs (i.e., the slope of single cell activation curves; GC in gray, PC in magenta) plotted against threshold input strength. Error bars indicate s.e.m..

(G) Summary plot of the gain of individual GCs and PCs. Error bars indicate s.e.m. Numbers of cells are given in parentheses. Error bars indicate s.e.m.; ns indicates nonsignificance, $p > 0.05$.



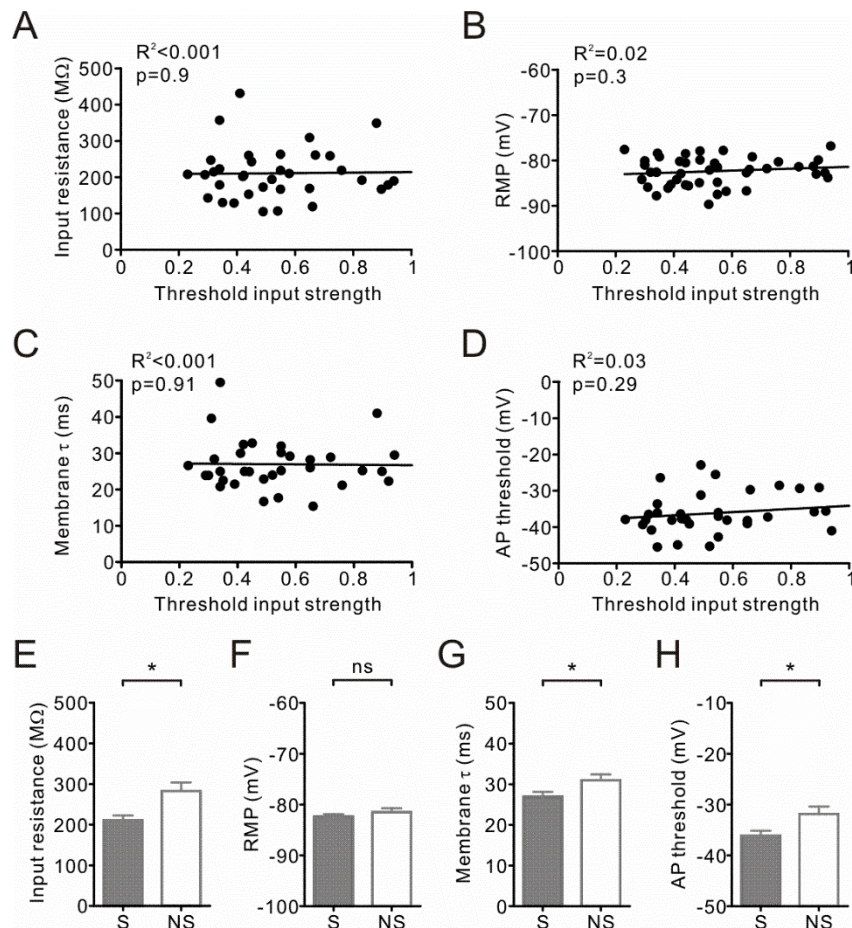


Fig. 5 Intrinsic properties of spiking and non-spiking GCs from adolescent rats

(A) Input resistance plotted against threshold input strength of GCs ($n = 35$).

(B) Resting membrane potential (RMP) plotted against threshold input strength for the same set of GCs illustrated in (A).

(C) Membrane τ plotted against threshold input strength for the same set of GCs illustrated in (A).

The membrane τ was measured by fitting a single exponential to the late portion of the membrane potential relaxation from a step current injection of 100 pA.

(D) Threshold potential for spike generation (AP threshold) plotted against threshold input strength for the same set of GCs illustrated in (A). Spike threshold was determined for APs triggered by a 100–

200 pA square current pulse. Spike threshold was defined as the potential of the membrane at the time at which the first-derivative of the membrane potential exceeded 50 mV/ms.

(E-H) Comparisons of input resistance, RMP, membrane τ , and AP threshold between S and NS GCs.

Error bars indicate s.e.m. * and ns indicate $p < 0.05$ and nonsignificance, respectively.



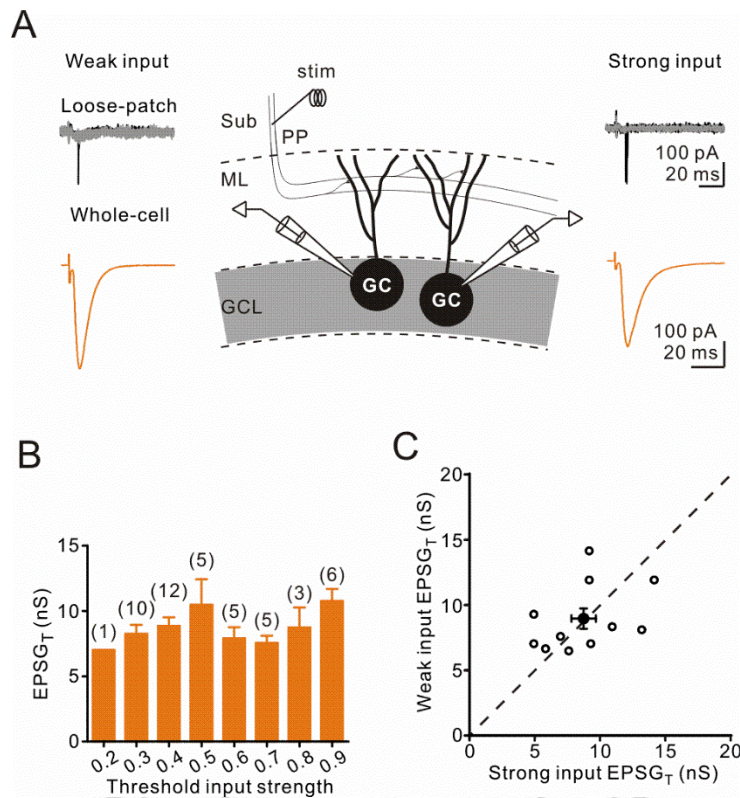


Fig. 6 Threshold excitatory inputs show no difference in GCs recruited at weak input or strong input

(A) Schematic of recording configuration. Top traces, example responses of two GCs simultaneously or sequentially recorded in loose patch to PP stimulation at threshold input strength (5 superimposed sweeps; successes are shown in black, failures in gray). The left GC was recruited at a weaker stimulus (threshold input strength = 0.3) than the right GC (threshold input strength = 0.7). Synaptic currents were subsequently measured by whole-cell recordings in individual cells. Bottom traces, the representative traces of threshold excitatory postsynaptic current (EPSC_{TS}; orange; i.e., EPSCs recorded at threshold input strength, average of 10 to 15 sweeps) recorded from the same cells voltage clamped at -75 mV.

(B) Summary plot of EP_{SG_T} ($n = 47$) versus threshold input strength. Error bars indicate s.e.m.

Numbers of GCs within the same threshold input strength range are shown on the top of each bar.

(C) Plot of EP_{SG_T} of GCs recruited at weak input strength (Weak input EP_{SG_T}) against EP_{SG_T} of

GCs recruited at strong input strength (Strong input EP_{SG_T} ; open circles, individual data; filled circle,

average of all data; dashed line indicates the unity line). Error bars indicate s.e.m.



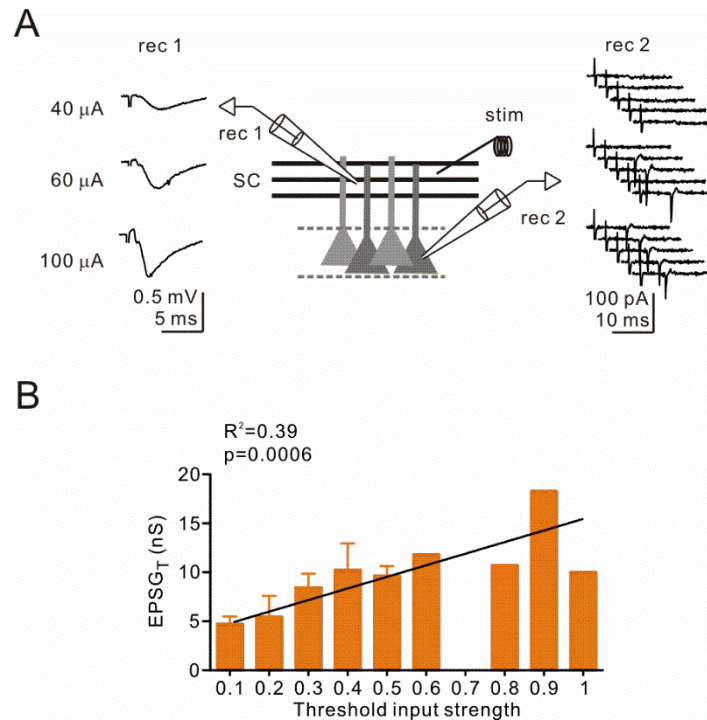


Fig. 7 The EPST_Ts are larger in CA1 PCs recruited at stronger input strength

(A) Schematic of recording configuration: a stimulation electrode (stim) was placed in the stratum radiatum of the CA1 region to activate Schaffer collaterals (SCs) from the hippocampal CA3 region; a field recording electrode (rec 1) was placed in the stratum radiatum to monitor the fEPSP; a cell-attached recording (rec 2) was made from a PC. Example traces of action currents (right, 5 consecutive sweeps) in the cell-attached configuration recorded from a PC and fEPSPs (left) in field recordings in response to SC stimulation at three different stimulus intensities.

(B) Summary plot of EPST_T (n = 26) against input strength at threshold. Black line indicates the linear fit to the data. Error bars indicate s.e.m.

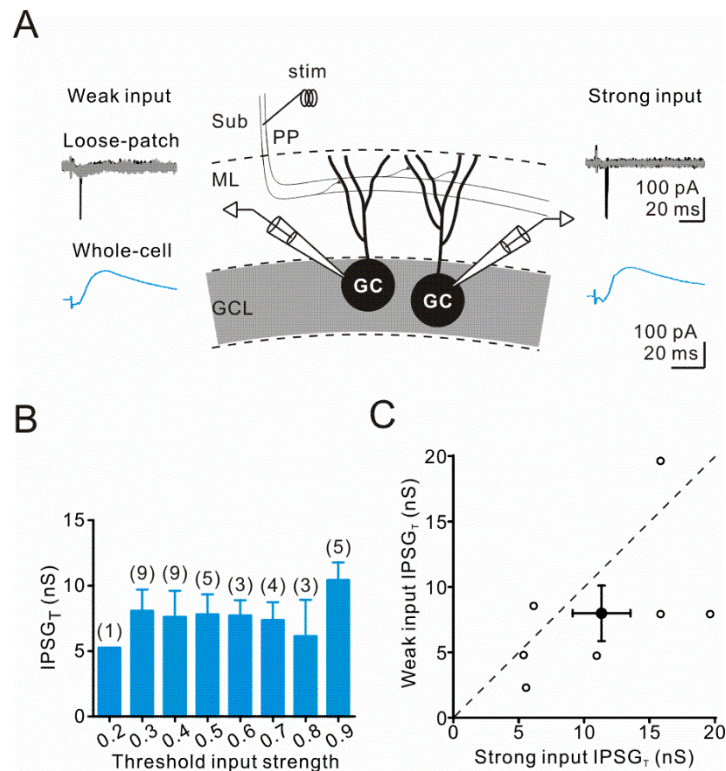


Fig. 8 Threshold inhibitory inputs to the GCs recruited at weak input are similar to the GCs recruited at strong input

(A) Schematic of recording configuration. Top traces, example responses of two GCs simultaneously or sequentially recorded in loose patch to PP stimulation at threshold input strength (5 superimposed sweeps; successes are shown in black, failures in gray). The left GC was recruited at a weaker stimulus (threshold input strength = 0.3) than the right GC (threshold input strength = 0.7). Synaptic currents were subsequently measured by whole-cell recordings in individual cells. Bottom traces, the representative traces of concomitantly evoked feedforward/feedback threshold inhibitory postsynaptic current (IPSC_T) recorded at -55 mV from the same cells (blue; isolated by subtraction from average of 10 to 15 sweeps).

(B) Summary plot of $IPSG_T$ ($n = 39$) against threshold input strength. Error bars indicate s.e.m.

Numbers of GCs within the same threshold input strength range are shown on the top of each bar.

(C) Plot of $IPSG_T$ of GCs recruited at weak input strength (Weak input $IPSG_T$) against $IPSG_T$ of GCs recruited at strong input strength (Strong input $IPSG_T$; open circles, individual data; filled circle, average of all data; dashed line indicates the unity line). Error bars indicate s.e.m.



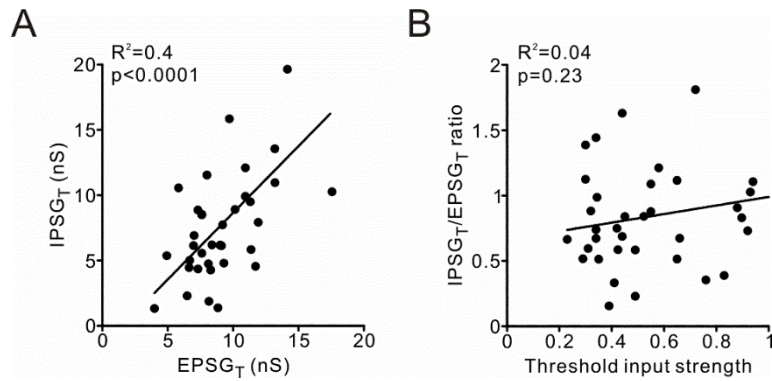
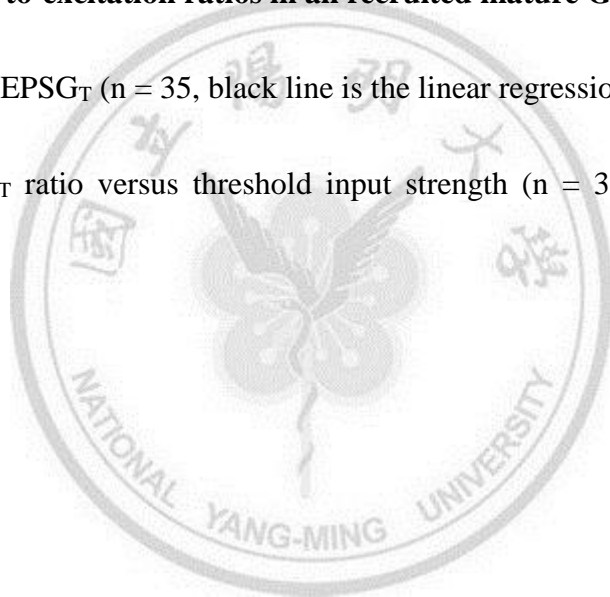


Fig. 9 Similar inhibition-to-excitation ratios in all recruited mature GCs

(A) Plot of IPST against EPST ($n = 35$, black line is the linear regression fit of the data).

(B) Plot of IPST/EPST ratio versus threshold input strength ($n = 35$, black line is the linear regression fit of the data).



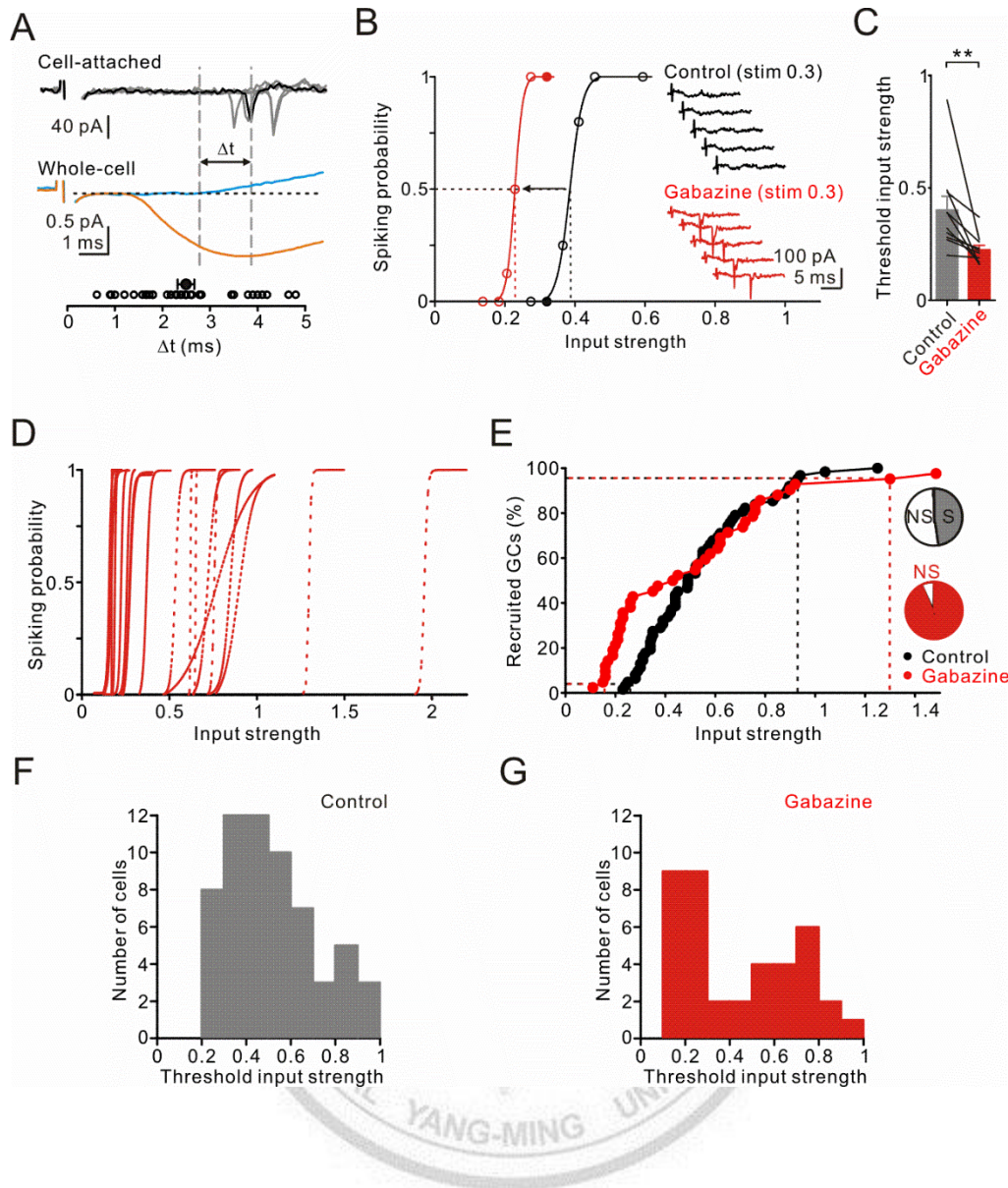


Fig. 10 GABA_A conductance restricts the dynamic range of the GC population

(A) Top traces represent cell-attached recordings from a single GC in response to threshold PP stimulation (5 superimposed sweeps). Bottom traces represent voltage-clamp recordings from the same neuron; the EPSC (orange, average of 10 sweeps) was recorded at -75 mV and the concomitant IPSC (blue, isolated by subtraction from average of 10 sweeps) was recorded at -55 mV. The left vertical dashed line indicates the onset of the IPSC and the right indicates the average spike timing

of the example GC. Bottom, summary of 37 experiments. The filled symbol represents the mean Δt .

Note that the GABAergic inhibition arrives before spike initiation in all recorded GCs.

(B) Spiking probability for one GC plotted against input strength before (black) and after (red) gabazine treatment (sigmoidal fit). Inset, loose-patch recording at 0.3 input strength before (black) and after (red) gabazine treatment, 5 consecutive sweeps for each condition. Filled symbols correspond to the example traces.

(C) Bar graph shows that gabazine treatment decreased the threshold input strength of spiking GCs. Gray and red bars show the average threshold input strength from GCs ($n = 10$) before and after gabazine treatment, respectively. Error bars indicate s.e.m. $**p < 0.01$.

(D) Continuous sigmoids indicate the spiking probability of the spiking GCs ($n = 10$) plotted against input strength after gabazine treatment. Dashed sigmoids indicate the spiking probability of the spiking GCs ($n = 10$), which were non-spiking GCs before gabazine treatment.

(E) Population activation curves in control conditions (black, data from Fig. 3C) and in gabazine (red, $n = 42$). Dashed lines demonstrate input strengths recruiting 5% and 95% of each population. The pie charts show the percentage of spiking (S) and non-spiking (NS) GCs under PP stimulation before (top) and after gabazine treatment (bottom), respectively.

(F) The histograms show the distribution of GCs with different threshold input strengths in control conditions.

(G) The histograms show the distribution of GCs with different threshold input strengths in gabazine

(red). Note that the distribution of threshold input strength shows two subpopulations after gabazine treatment.



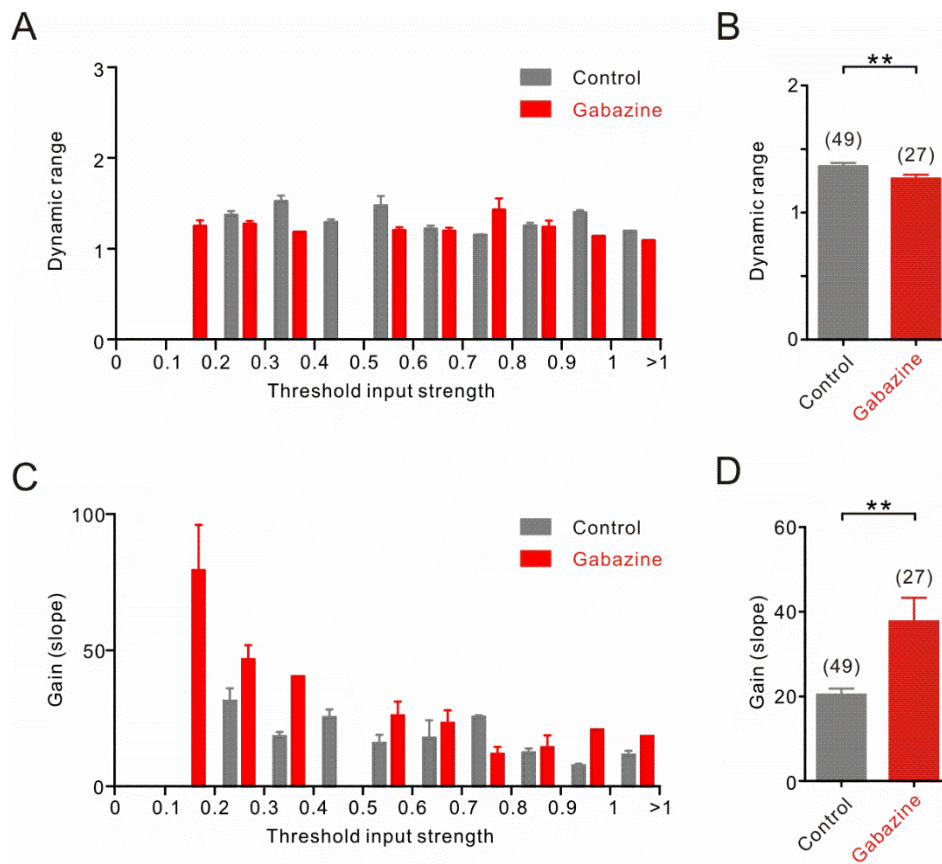


Fig. 11 The dynamic range and gain of individual GCs are also modulated by GABAergic inhibition

(A) The bar graph shows the dynamic range of individual GCs in the control condition and in gabazine (gray, control; red, gabazine) plotted against threshold input strength. Error bars indicate s.e.m.

(B) Summary plot of the dynamic range of individual GCs in the control condition (gray) and in gabazine (red). Error bars indicate s.e.m.; ** indicates $p < 0.01$.

(C) The bar graph shows the gain of individual GCs in control conditions and in gabazine (gray, control; red, gabazine) plotted against threshold input strength. Error bars indicate s.e.m.

(D) Summary plot of the gain of individual GCs in control conditions (gray) and in gabazine (red).

Error bars indicate s.e.m.; ** indicates $p < 0.01$.



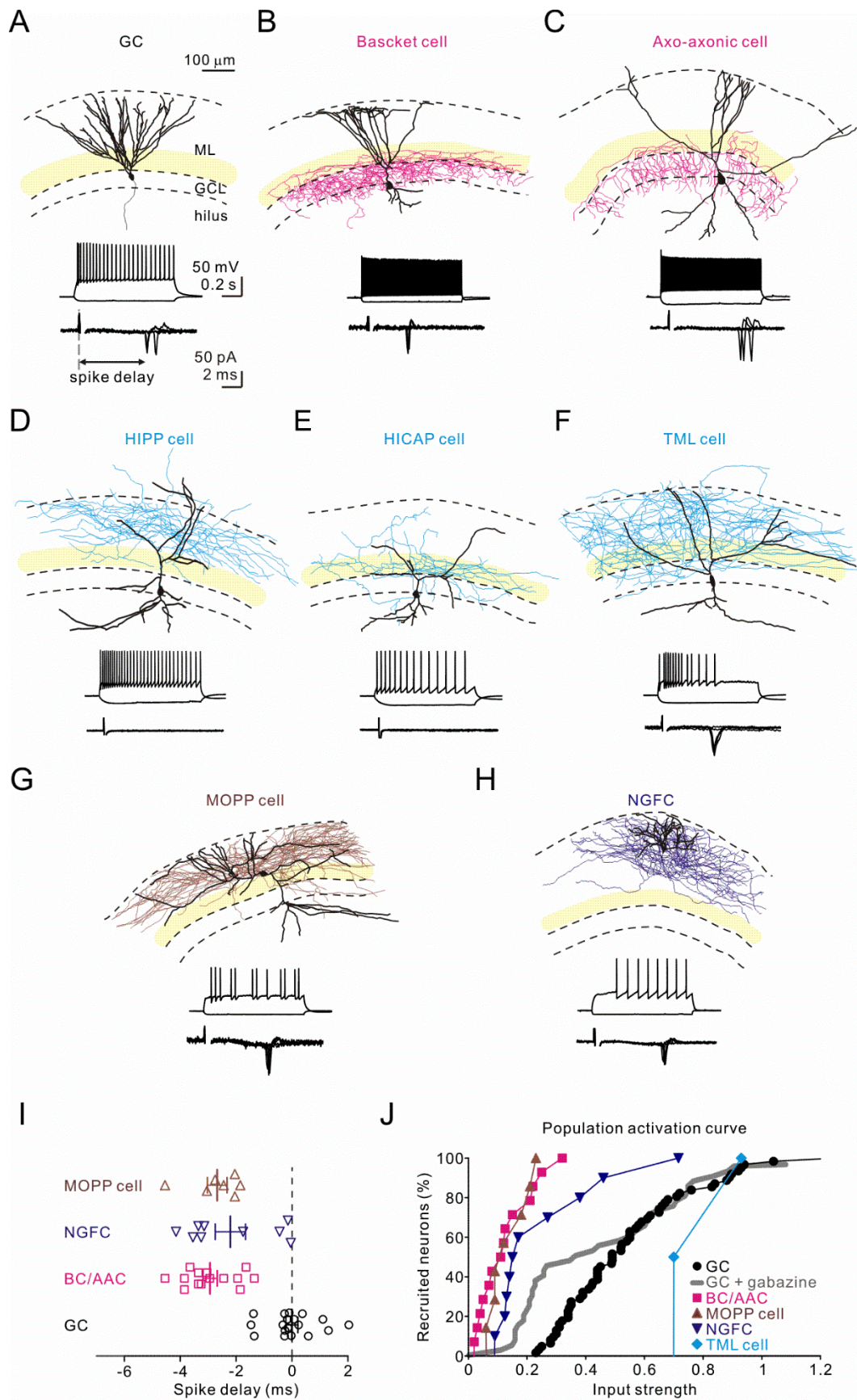


Fig. 12 Regulation of the GC population dynamic range by somatic interneuron (INs) and ML

INs

(A-H) Reconstruction (top), spiking pattern (middle), and cell-attached recording traces (bottom) from eight representative cells. From left to right: (A) GC, which displayed GC morphology; (B) Basket cell (BC), which showed fast spiking firing properties (> 150 Hz) and had characteristically basket-like dense axonal arborization (pink) within the granule cell layer (GCL); (C) Axo-axonic cell (AAC), which also show fast spiking firing patterns but projected its axons (pink) in a parallel manner into the granule cell layer (GCL); (D) hilar PP-associated (HIPP) cell, which had the axonal distribution in the PP terminal field (pale blue); (E) hilar commissural-associational (HICAP) cell, which had the main axonal innervation (pale blue) in the inner molecular layer (pale yellow); (F) total molecular layer (TML) cell, which had the axonal innervation (pale blue) in both inner molecular layer (pale yellow) and outer molecular layer; (G) ML PP-associated (MOPP) cell, which had soma in the ML and dense axonal arborization (brown) in the ML; (H) neurogliaform cell (NGFC), which had soma and small dendritic trees in the ML and axonal innervation covering the outer-third and middle-third of the ML (blue). Somata and dendrites are indicated in black. Dashed lines mark the margins of the hilus, GCL, and ML from bottom to top. BCs and AACs exhibited a fast-spiking firing pattern; HIPP, HICAP, TML, and MOPP cells displayed non-fast spiking patterns; NGFCs exhibited a late-firing pattern. Cell-attached recordings show spikes, detected as action currents (5 superimposed sweeps), evoked at threshold input strength of each neuron. Note that HIPP ($n = 6$),

HICAP ($n = 7$), and two of TML ($n=2/4$) cells cannot be recruited by the maximal input strength.

(I) Spike delay in response to PP stimulation delivered at 0.5 input strength in GCs (black, $n = 18$),

BCs/AACs (pink, $n = 14$), MOPP cells (brown, $n = 7$), and NGFCs (blue, $n = 9$).

(J) Population activation curves for BCs/AACs (square, $n = 14$), MOPP cells (triangle, $n = 7$), NGFC

cells (inverted triangle, $n = 10$), TML cells (diamond, $n=2/4$), and GCs (circle, $n = 62$, from Fig. 3C).

The gray line represents the data from GCs in gabazine.



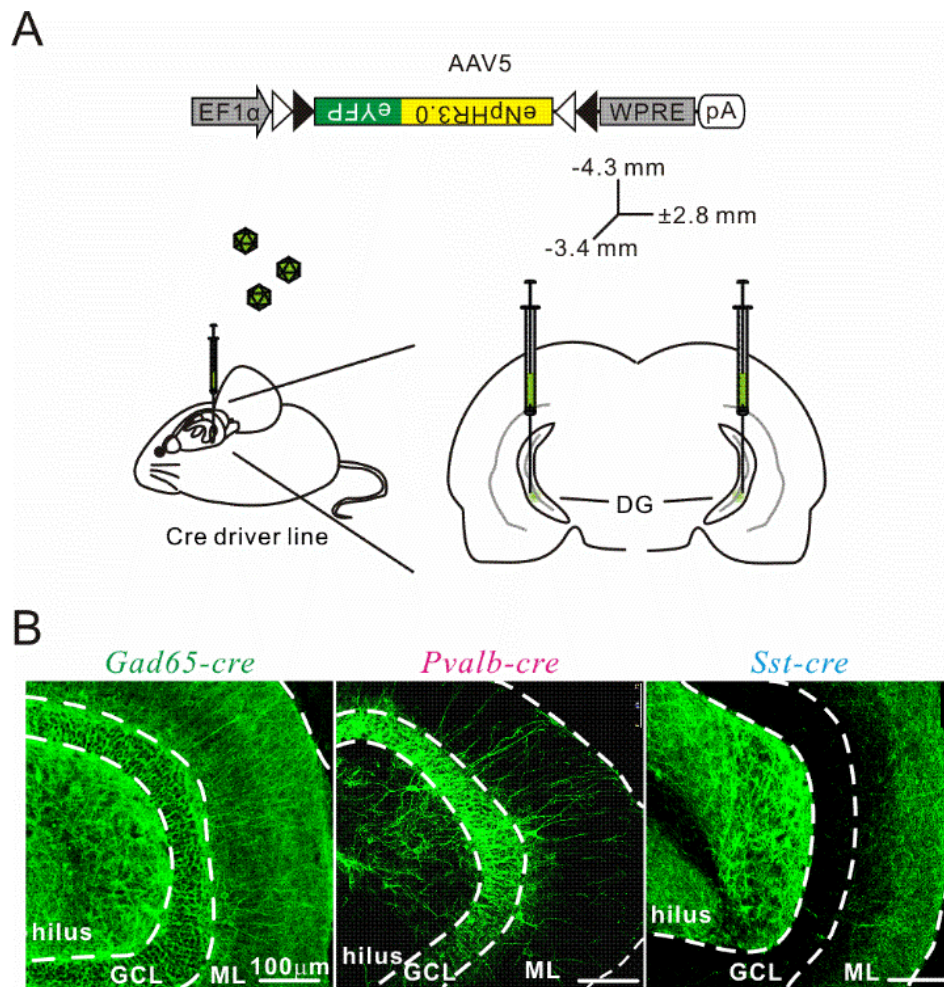


Fig. 13 Expression patterns of eNpHR3.0-eYFP in the ventral DG in cre-expressing mice

(A) Schematic of a mouse brain injected with an AAV5 carrying EF1 α -DIO-eNpHR3.0-eYFP into the ventral hippocampal DG.

(B) Left to right, two-photon image stacks of the ventral DG from *Gad65-cre*, *Pvalb-cre*, and *Sst-cre* mice 6 weeks after virus injection. Note that the green fluorescent signals were observed in all layers of the DG in *Gad65-cre* mice, but mostly detected in the GCL of *Pvalb-cre* mice and in the ML and hilus of *Sst-cre* mice.

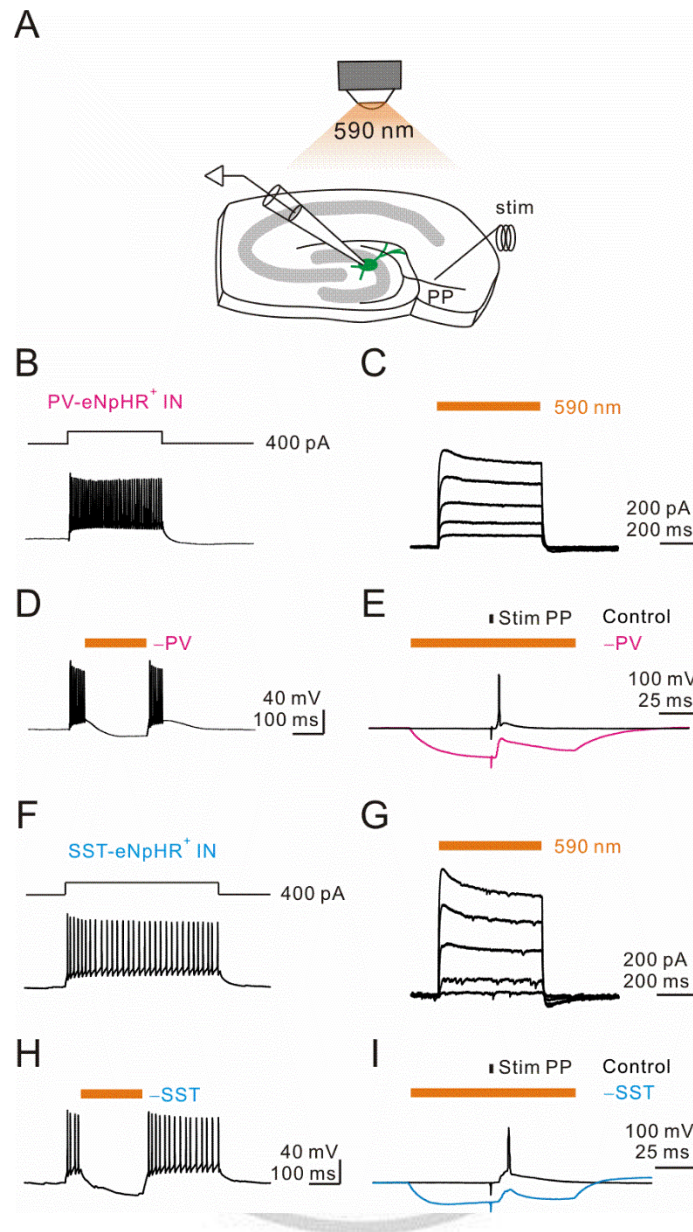


Fig. 14 Expression of eNpHR can selectively silence specific types of INs in DG

(A) Schematic of recording configuration: a stimulation electrode was placed in the Sub to activate the PP; an eNpHR-eYFP positive IN was whole-cell patch clamped by a recording electrode. The amber light was delivered through the microscope objective during PP stimulation.

(B) Firing patterns of a PV-eNpHR⁺ IN evoked by current pulse injection.

(C) Light evoked currents were recorded in a PV-eNpHR⁺ IN at five different light intensities. Orange

bars in (C,D, E,G,H,I) indicate the duration of light.

(D) Example spikes evoked by current pulse injection as in (B) in a PV-eNpHR⁺ IN in the presence of optogenetic silencing.

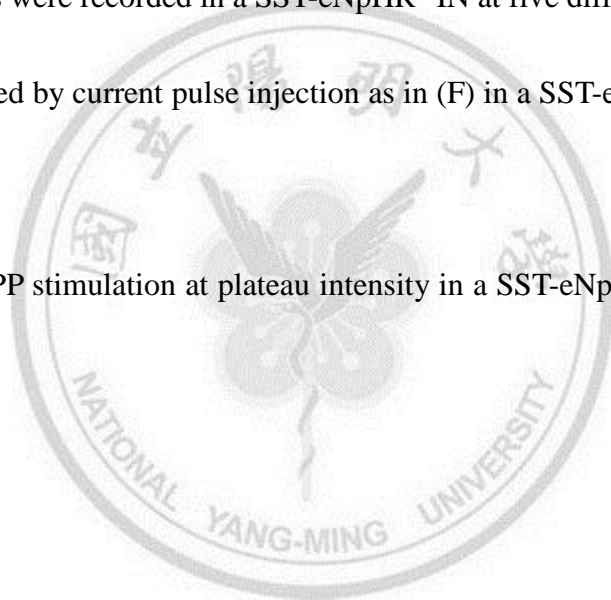
(E) The spike evoked by PP stimulation at plateau intensity in a PV-eNpHR⁺ IN could be inhibited by light.

(F) Firing patterns of a SST-eNpHR⁺ IN evoked by current pulse injection.

(G) Light evoked currents were recorded in a SST-eNpHR⁺ IN at five different light intensities.

(H) Example spikes evoked by current pulse injection as in (F) in a SST-eNpHR⁺ IN in the presence of optogenetic silencing.

(I) The spike evoked by PP stimulation at plateau intensity in a SST-eNpHR⁺ IN could be inhibited by light.



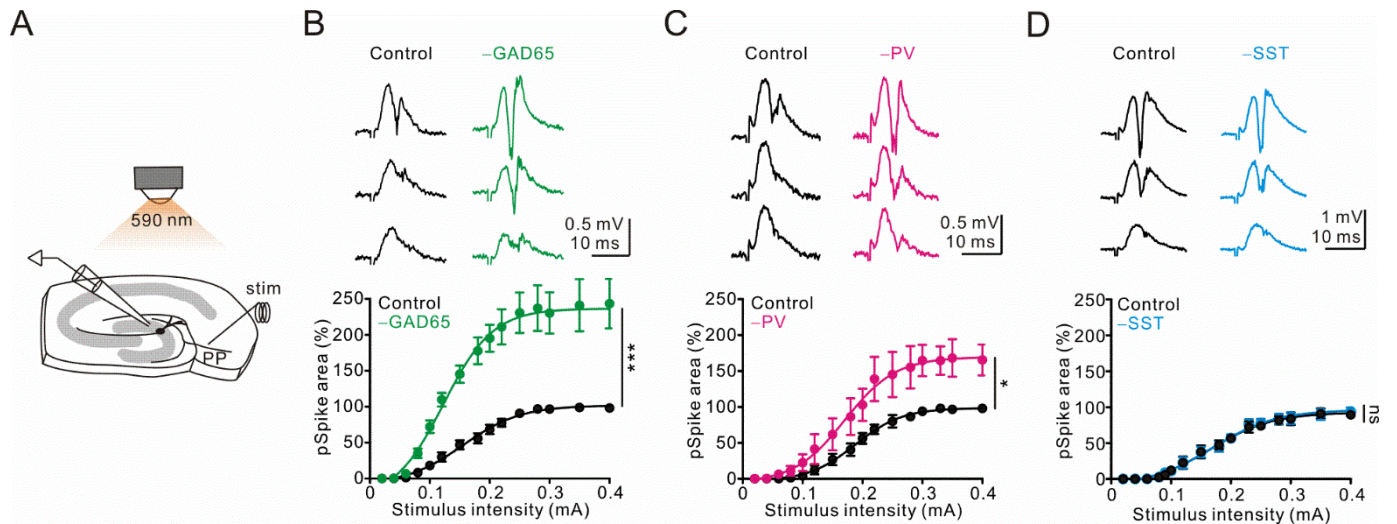


Fig. 15 Parvalbumin-expressing (PV⁺) INs regulate GC input-output (I-O) transformations

(A) Schematic of recording configuration: a stimulation electrode was placed in the Sub to activate the PP; a field recording electrode was placed in the GCL to monitor the population spike (pSpike). The amber light was delivered through the microscope objective during PP stimulation.

(B) Top, field recordings of pSpikes (denoted by the downward deflection) from the GCL in control conditions (black, left) or under light stimulation (-GAD65; green, right) at three different stimulus intensities in *Gad65-cre* mouse. Bottom, the pSpike area is plotted against stimulus intensity under control conditions (black) or under light stimulation (green) in *Gad65-cre* mice (sigmoidal fit to the data-points). Note the pSpike is greatly increased during light stimulation at all stimulus intensities.

Error bars indicate s.e.m. *** $p < 0.001$

(C) Top, the same experimental configuration as in (B) was used for *Pvalb-cre* mice. Bottom, the pSpike area is plotted against stimulus intensity under control conditions (black) and under light stimulation (pink) in *Pvalb-cre* mice. * $p < 0.05$.

(D) Top, the same experimental configuration as in (B) was used for *Sst-cre* mice. Bottom, the area of the pSpike is plotted against stimulus intensity under control conditions (black) or under light stimulation in *Sst-cre* mice (pale blue). Note the pSpike during light stimulation was the same as that in control conditions at any given stimulus intensity in *Sst-cre* mice. ns indicates nonsignificance.



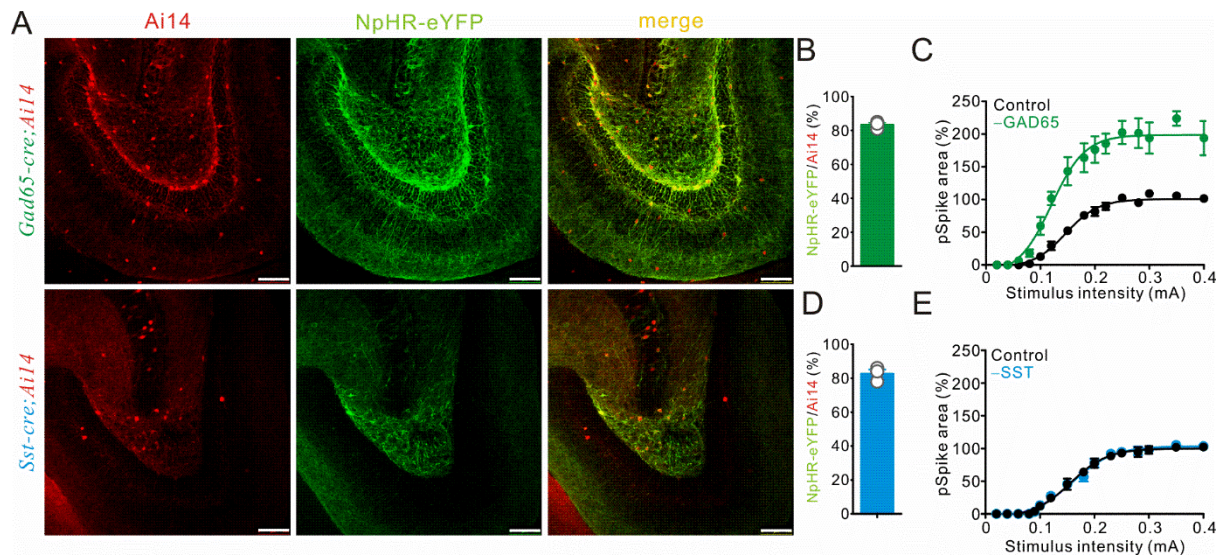


Fig. 16 The lack of effect of silencing SST⁺ INs on DG pSpike is not due to poor expression efficiency of NpHR-eYFP

(A) Confocal image stacks of the ventral DG from *Gad65*-(top) and *Sst-cre/Ai14*(bottom) mice 6 weeks after virus injection. Scale bar, 100 μ m.

(B) The expression efficiency of NpHR-eYFP in *Gad65*-(top) and *Sst-cre/Ai14*(bottom) mice.

(C) The pSpike area is plotted against stimulus intensity under control conditions (black) or under light stimulation (green) in *Gad65-cre/Ai14* mice (sigmoidal fit to the data-points). Note the pSpike is greatly increased during light stimulation at all stimulus intensities.

(D) The area of the pSpike is plotted against stimulus intensity under control conditions (black) or under light stimulation in *Sst-cre/Ai14* mice (pale blue). Note the pSpike during light stimulation was the same as that in control conditions at any given stimulus intensity in *Sst-cre/Ai14* mice.

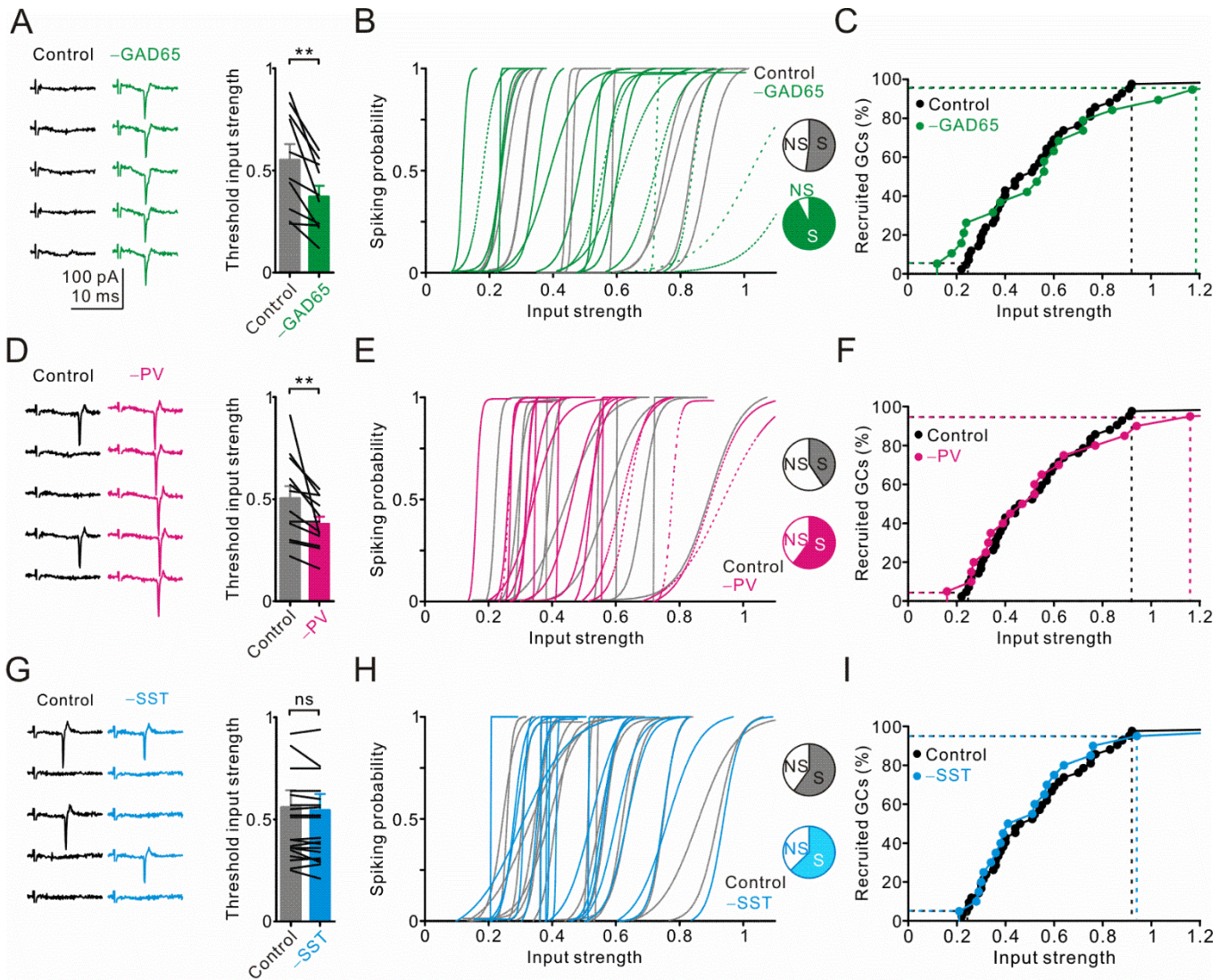


Fig. 17 Silencing of PV⁺ INs, but not SST⁺ INs, expands the dynamic range of the GC population

(A) Cell-attached recordings from a single GC before (black, left) during light stimulation (green, right) at threshold input strength in *Gad65-cre* mouse. Summary plot of threshold input strengths from GCs ($n = 10$) without and with light stimulation in *Gad65-cre* mice, respectively. Bars represent mean values; circles connected by lines represent data from the same experiment. Error bars indicate s.e.m. $**p < 0.01$.

(B) Gray continuous sigmoids indicate the spiking probability of the spiking GCs ($n = 10$) in control

conditions. Green continuous and dashed sigmoids indicate the spiking probability of the spiking GCs (n = 10) and GCs, which are NS in control conditions (n = 9), respectively, during light stimulation.

(C) Activation curves in control conditions (black, n = 41) and under light stimulation (green, n = 19).

Dashed lines indicate input strengths recruiting 5% and 95% of the GC population. Note that silencing of GAD65⁺ INs expanded the dynamic range of the GC population.

(D) Cell-attached recordings from a single GC before (black, left) and during light stimulation (pink, right) at threshold input strength in *Pvalb-cre* mouse. Summary plot of threshold input strengths from

GCs (n = 12) with and without light stimulation in *Pvalb-cre* mice, respectively. Error bars indicate s.e.m. Note that optogenetic silencing of PV⁺ INs decreased the threshold input strength of spiking GCs.

(E) Gray continuous sigmoids indicate the spiking probability of the spiking GCs (n = 12) without light stimulation. Pink continuous and dashed sigmoids indicate the spiking probability of the spiking GCs (n = 12) and non-spiking GCs (n = 6), respectively, with light stimulation.

(F) Activation curves in control conditions (black, n = 41) and under light stimulation (pink, n = 20).

(G) Cell-attached recordings from a single GC before (black, left) and during light stimulation (pale blue, right) at threshold input strength in *Sst-cre* mouse. Pale blue and black bars show the threshold

input strengths from GCs (n = 19) with and without light stimulation in *Sst-cre* mice, respectively.

Error bars indicate s.e.m. Note that silencing SST⁺ INs did not change the threshold input strength of recruited GCs.

(H) Gray sigmoids indicate the spiking probability of GCs ($n = 19$) which could be recruited without light stimulation. Pale blue sigmoids indicate the spiking probability of GCs ($n = 19$) with light stimulation.

(I) Activation curves before (black, $n = 41$) and during light stimulation (pale blue, $n = 20$).



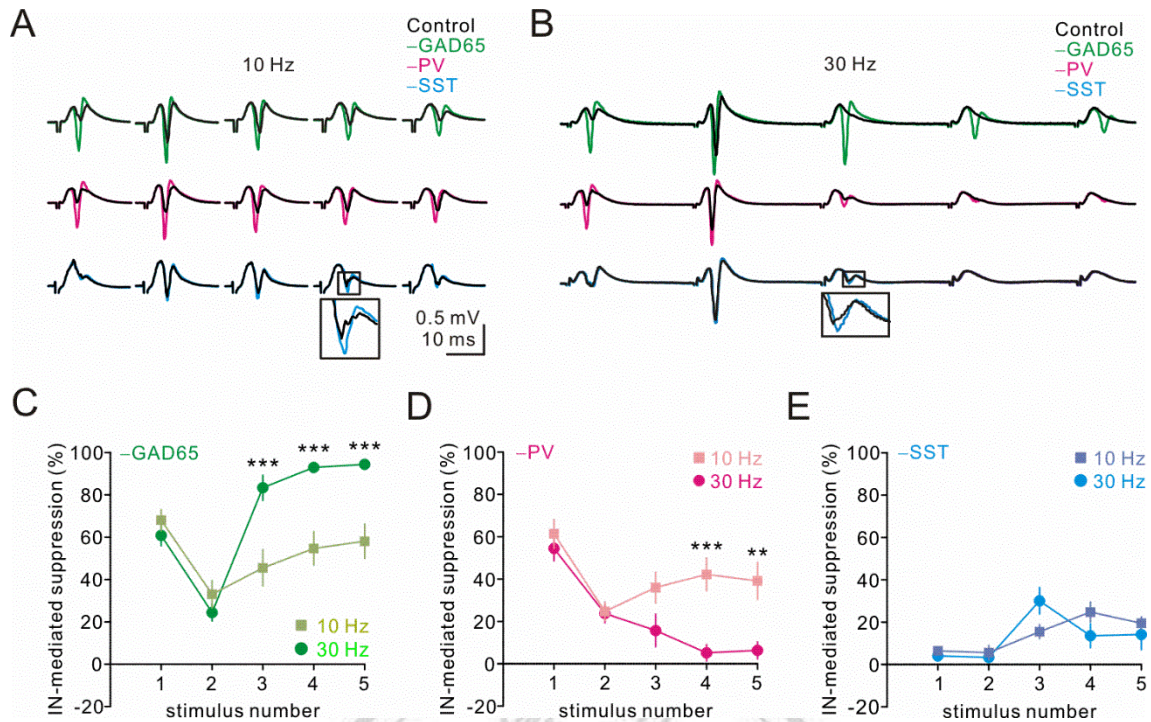


Fig. 18 PV⁺ and SST⁺ INs differentially regulate the pSpike series in the GC population

(A) From top to bottom, pSpikes were evoked by PP stimulation at 10-Hz trains before (black) and after silencing of GAD65⁺ (-GAD65, green), PV⁺ (-PV, pink), and SST⁺ (-SST, pale blue) neurons. Plateau stimulation intensity was used to evoke maximal pSpikes. Amber light was illuminated during trains. The insets show the enlargement of the traces in the square. (B) From top to bottom, pSpikes were evoked by PP stimulation at 30-Hz (right) trains before (black) and after silencing of GAD65⁺ (-GAD65, green), PV⁺ (-PV, pink), and SST⁺ (-SST, pale blue) neurons. Plateau stimulation intensity was used to evoke maximal pSpikes. Amber light was illuminated during trains. The insets show the enlargement of the traces in the square.

(C–E) Summary plots of GAD65⁺, PV⁺, and SST⁺ IN-mediated suppression versus stimulus number.

IN-mediated suppression (%) is quantified by $100 \times (\text{pSpike}_{\text{IN}} - \text{pSpike}_{\text{Control}}) / \text{pSpike}_{\text{IN}}$. We used

two-way repeated-measures ANOVA to compare 10 Hz versus 30 Hz across multiple stimulus numbers; *post hoc* Bonferroni's test was used to test the significance between 10 Hz and 30 Hz at each stimulus number.



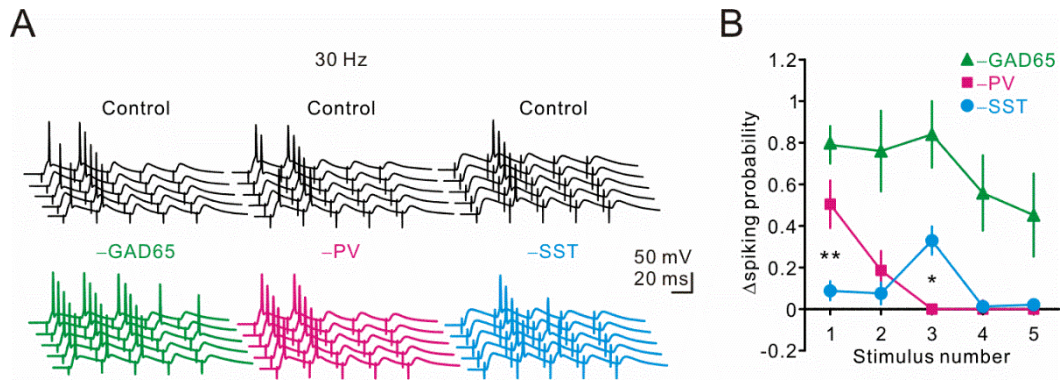


Fig. 19 PV⁺ and SST⁺ INs differentially regulate the pSpike series in the individual GCs

(A) From left to right, whole-cell current-clamp recordings from GCs in response to PP stimulation at near-threshold strength before (top, black) and after optogenetic silencing of GAD65⁺ (green), PV⁺ (pink) and SST⁺ (pale blue) INs.

(B) Summary plot of Δ spiking probability in GCs against stimulus number following silencing of GAD65⁺ (green), PV⁺ (pink) and SST⁺ (pale blue) INs.

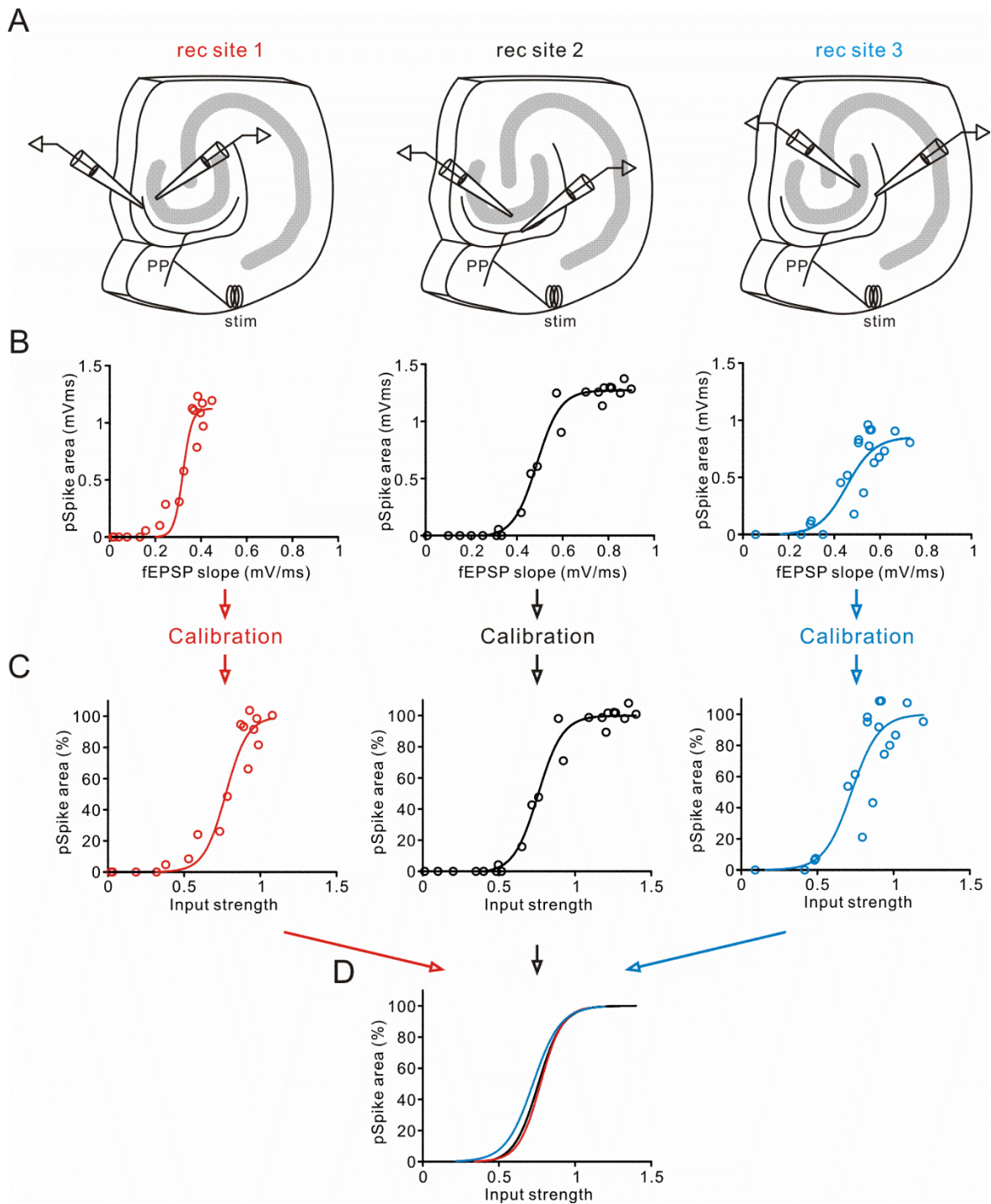


Fig. 20 Calibration of cortical input strength from different recording sites in the same slice

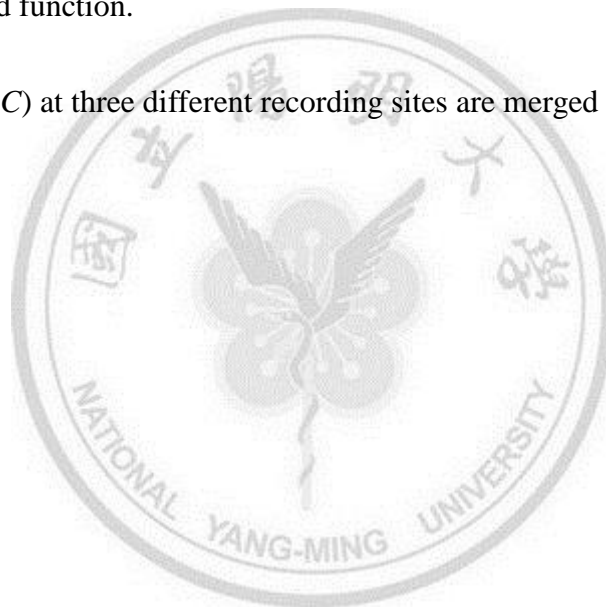
(A) Schematic of recording configuration: Left, a stimulation electrode (stim) was placed in the Sub to activate the PP fibers; two field recording electrodes were placed in the GCL and in the ML to

simultaneously detect the pSpike and fEPSP in response to single pulse delivered to the PP at varying stimulus strengths. After calibration, the two recording electrodes were simultaneously moved to the other recording sites (middle and right) for comparing the effects of calibrations.

(B) The pSpike area is plotted against fEPSP slope for the experiment illustrated in (A) at three indicated recording sites. Data are fit with a sigmoid function.

(C) The normalized pSpike area is plotted against input strength for the same experiments as in (B). Data are fit with a sigmoid function.

(D) The fitting curves in (C) at three different recording sites are merged together in the same plot.



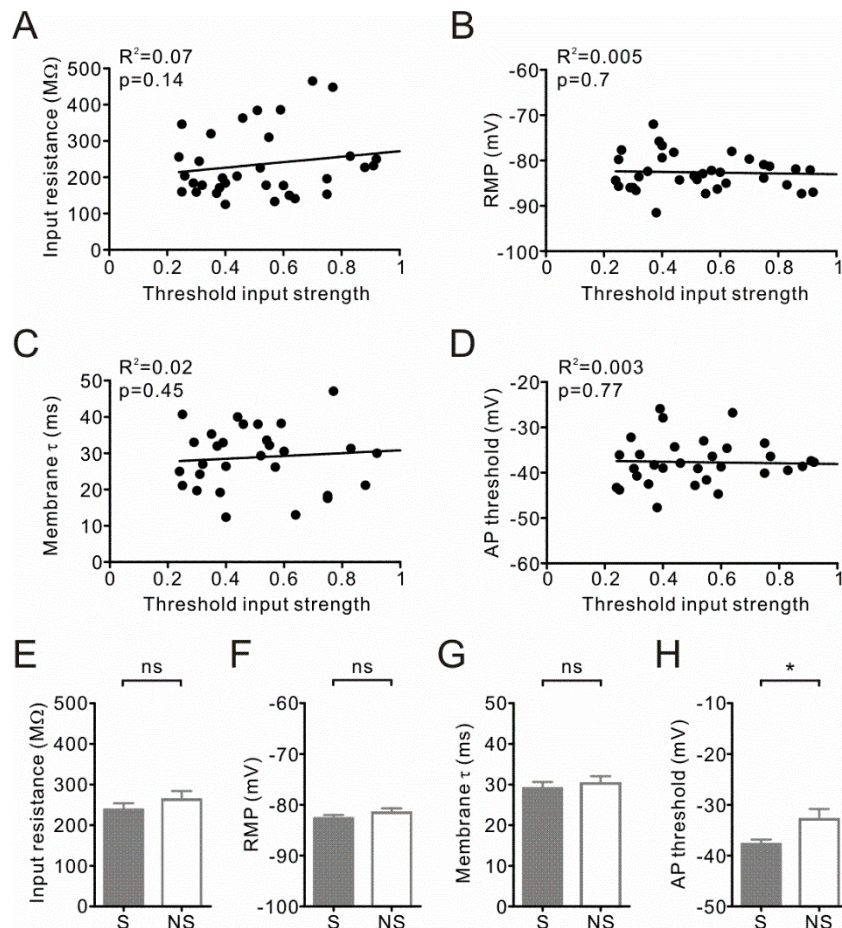


Fig. 21 Intrinsic properties of spiking and non-spiking GCs from adult mice

(A) Input resistance plotted against threshold input strength of GCs ($n = 33$).

(B) RMP plotted against threshold input strength for the same set of GCs illustrated in (A).

(C) Membrane τ plotted against threshold input strength for the same set of GCs illustrated in (A).

The membrane τ was measured by fitting a single exponential to the late portion of the membrane potential relaxation from a step current injection of 100 pA.

(D) AP threshold plotted against threshold input strength for the same set of GCs illustrated in (A).

Spike threshold was determined for APs triggered by a 100–200 pA square current pulse. Spike threshold was defined as the potential of the membrane at the time at which the first-derivative of the

membrane potential exceeded 50 mV/ms.

(E–H) Comparisons of input resistance, RMP, membrane τ , and AP threshold between S and NS GCs.

Error bars indicate s.e.m. * and ns indicate $p < 0.05$ and nonsignificance, respectively.



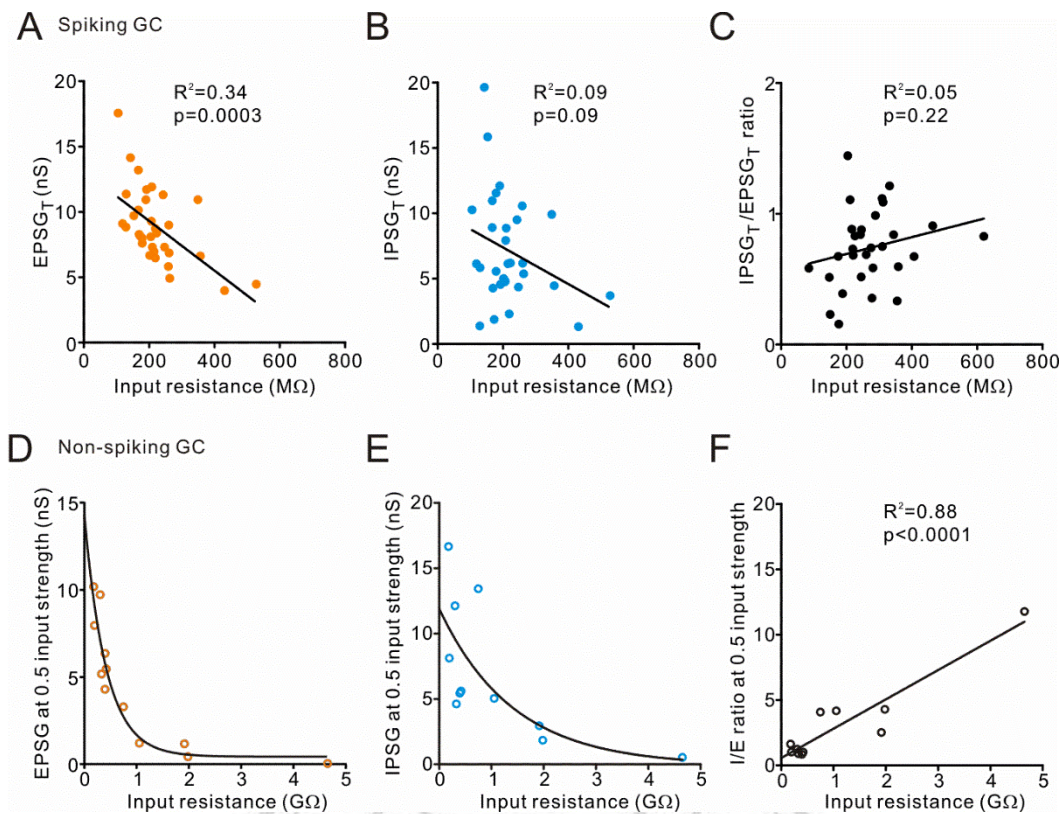


Fig. 22 EPSP_T negatively correlates with GC input resistance

(A) EPSP_T is plotted against input resistance for spiking GCs (n = 32).

(B) IPSP_T plotted against input resistance for spiking GCs (n = 30).

(C) The ratio of IPSP_T to EPSP_T plotted against input resistance for spiking GCs (n = 30).

(D) EPSP at 0.5 input strength is plotted against input resistance for non-spiking GCs (n = 12).

(E) IPSP at 0.5 input strength plotted against input resistance for non-spiking GCs (n = 11).

(F) The ratio of IPSP to EPSP at 0.5 input strength plotted against input resistance for non-spiking GCs (n = 11). Note some of non-spiking GCs had high input resistance, indicating non-mature GCs.

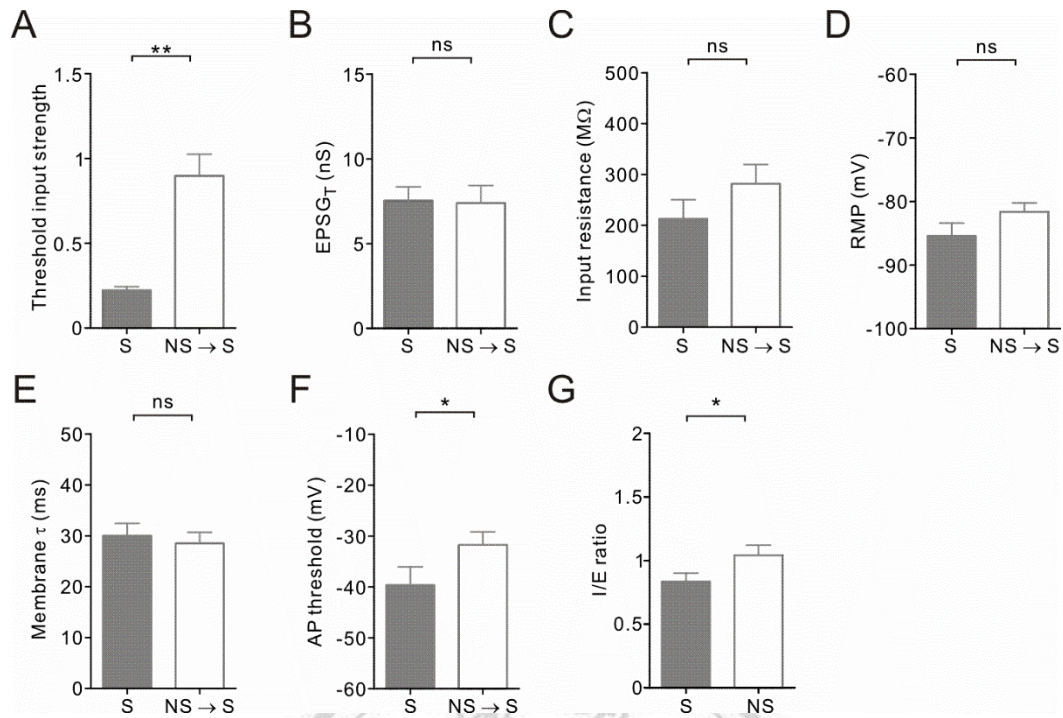


Fig. 23 Comparison of functional properties between spiking (S) GCs and NS→S GCs, which transformed into spiking GCs after gabazine treatment

(A) Summary of threshold input strength (n = 10 for S, n = 10 for NS→S). ** indicates $p < 0.01$.

(B) Summary of EPSC_T (n = 3 for S, n = 5 for NS→S). ns indicates nonsignificance.

(C) Summary of input resistance (n = 10 for S, n = 10 for NS→S). ns indicates nonsignificance.

(D) Summary of RMP (n = 9 for S, n = 10 for NS→S). ns indicates nonsignificance.

(E) Summary of membrane τ (n = 9 for S, n = 10 for NS→S). ns indicates nonsignificance.

(F) Summary of AP threshold (n = 9 for S, n = 10 for NS→S). * indicates $p < 0.05$.

(G) I/E ratio of spiking (S) GCs (n = 35) versus non-spiking (NS) GCs (n = 12), which spiked in response to PP stimulation after addition of gabazine. Note that I/E ratios were measured before gabazine treatment. Error bars indicate s.e.m. * indicate $p < 0.05$.

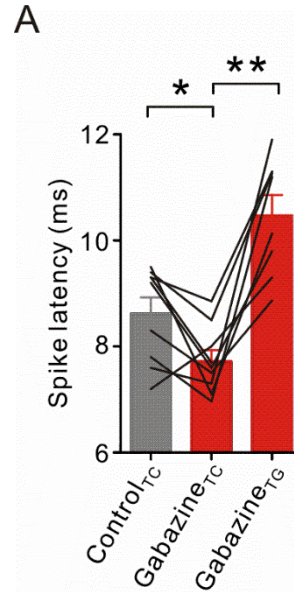


Fig. 24 GABAergic inhibition regulates spike latency in GCs

(A) Comparisons of GC spike latency at threshold stimulation in control conditions (Control_{Tc}, gray), in gabazine (Gabazine_{Tc}, red), and spike latency stimulated at threshold measured in gabazine (Gabazine_{TG}, red). Error bars indicate s.e.m. * indicates $p < 0.05$, ** indicates $p < 0.01$.

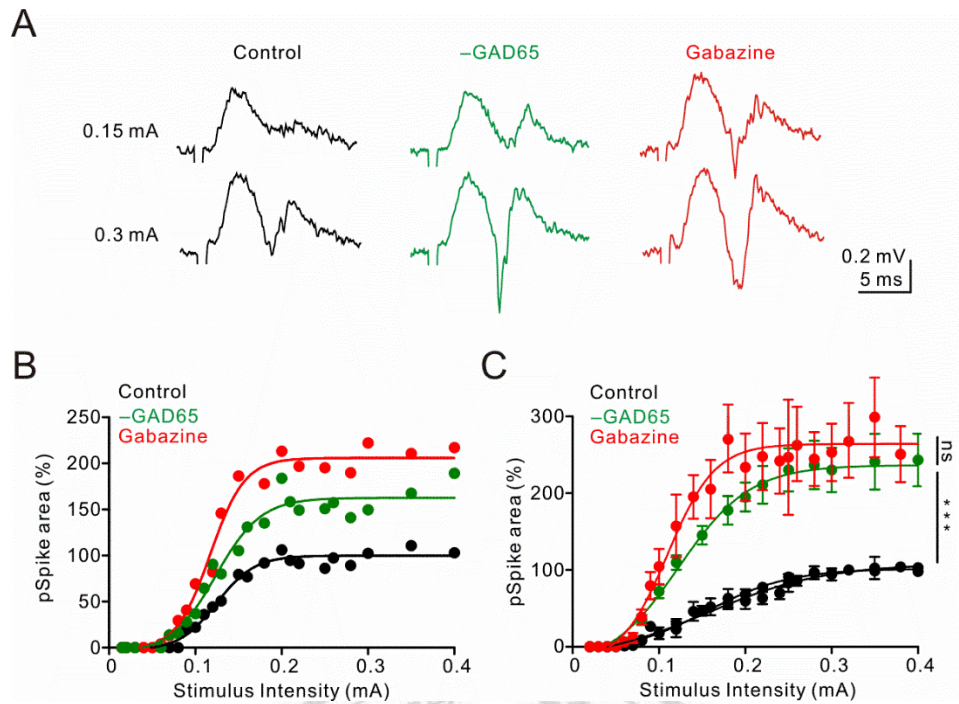


Fig. 25 The GC input-output (I-O) transformations in optogenetic silencing of GAD65⁺ INs are comparable to that in gabazine

(A) Field recordings of pSpikes from the GCL in control conditions (black, left), under light stimulation (-GAD65; green, middle), and in gabazine (red, right) at two different stimulus intensities in *Gad65-cre* mouse.

(B) The pSpike area is plotted against stimulus intensity in control conditions (black), under light stimulation (green), and in gabazine in the same slice as in (A) (sigmoidal fit to the data-points).

(C) Summary of the pSpike area plotted against stimulus intensity. Note the pSpike is greatly increased during light stimulation and gabazine treatment at all stimulus intensities. Error bars indicate s.e.m. *** $p < 0.001$

CURRICULUM VITAE

Cheng-Ta Lee

Ph.D.

Institute of Neuroscience

National Yang Ming University

Email: tsohchi@gmail.com

Last updated: 2015/7/15

Education

2009-now Ph.D., Institute of Neuroscience, National Yang Ming University, Taiwan.

2008-2009 M.S., Institute of Neuroscience, National Yang Ming University, Taiwan.

2002-2006 B.S., Life Science, National Tsing Hua University, Taiwan.

Awards, Fellowships, and Grants

MoST Travel Grant to Society for Neuroscience Annual Meeting, 2014

NSC Travel Grant to Society for Neuroscience Annual Meeting, 2010

Brief Synopsis of PhD Research:

In my major project in PhD, I used optogenetics and electrophysiological recordings to examine the inhibitory control of dynamic range of hippocampal dentate granule cell population. And I found that parvalbumin positive interneurons and somatostatin positive interneurons differentially regulate the dynamic range of dentate granule cells at various activation states. In the project collaborated with Dr. Chen's lab in Sinica, we examine the role of type 6 adenylyl cyclase (AC6) in hippocampus dependent learning and found that through decreasing expression of NR2B containing NMDA receptors, AC6 elevates the induction threshold of hippocampal LTD and attenuates reversal hippocampal learning.

Research Interests

The wiring and functional roles of hippocampal interneurons.

Employment

2010-2014 Part-time Research Assistant, Institute of Neuroscience, National Yang-Ming University.

2009 Volunteer of 'Typhoon-Morakot-caused flood' in Taiwan

2008 Volunteer of 'Saving the Tasmania Devil' in Australia.

2008 Volunteer of 'Conservation of wild dolphin' in Australia.

2008 House keeper in Australia.

2008 Group picker in Australia.

2006-2007 Military Services, Corporal of Marine, Taiwan.

2005 Restaurant waiter

Experimental techniques

Slice electrophysiology

Optogenetics

Immunohistochemistry staining

Morphology 3D reconstruction

Genotyping

Western blot

Stereotaxic injection

Interests

Tennis, traveling, singing, mountain hiking, river tracing

Conferences, Presentations and Courses Attended

Society for Neuroscience Annual Meeting, Washington D.C. November 15th - 19th 2014, presented poster.

Neuroscience Society of Taiwan Annual Meeting, Taiwan, October 25, 2013.

Joint Annual Conference of Biomedical Science, Taiwan, March 23-24, 2013, presented poster.

Taiwan-Poland Neuroscience Workshop on Brain Aging, Taiwan, December 6, 2012.

Society for Neuroscience Annual Meeting, New Orleans, LA. October 13-17, 2012.

Neuroscience Society of Taiwan Annual Meeting, Taiwan, September 22, 2012.

Frontiers in Neuroscience: From Genes to Cognition, Taiwan, October 23-24, 2010, presented poster.

Publications / Conference Papers (in reverse chronological order)

1. **CT Lee**, MH Kao and CC Lien. Specific Types of Interneurons Regulate Input Pattern-Dependent Recruitment of Dentate Granule Cells.

2. CP Chang, **CT Lee**, WS Ho, MS Lin, HL Lai, CL Chien, PL Cheng, CC Lien, and YJ Chern. Type VI Adenylyl Cyclase Modulates NMDAR Mediated Synaptic Plasticity. In preparation

(co-first author).

3. YY Huang, YC Liu, **CT Lee**, YC Lin, KY Chang, SH Chiou, CC Lien. Revisiting Lamotrigine-mediated effects on hippocampal GABAergic inhibition. In preparation.

4. TT Hsu, **CT Lee**, MH Tai and CC Lien (2015). Differential Recruitment of Dentate Gyrus Interneuron Types by Commissural Versus Perforant Pathways. **Cerebral Cortex** 2015 June online published.

5. **CT Lee** and CC Lien. (2014). Inhibitory Control of Dynamic Range of Hippocampal Dentate Granule Cell Population. Society for Neuroscience annual meeting.

6. **CT Lee** and CC Lien. (2013). Retrograde Synaptic Plasticity at Dentate Granule Cells. Joint Annual Conference of Biomedical Science in Taiwan.

7. **CT Lee**, CC Lien. (2010) M₂-like Muscarinic Acetylcholine Receptors Regulate Perisomatic GABA Release in Rat Dentate Gyrus. Society for Neuroscience annual meeting.

8. Chiang PH, Yeh WC, **Lee CT**, Huang YY, Lien CC (2010). M₁-like muscarinic acetylcholine receptors regulate fast-spiking interneuron excitability in rat dentate gyrus. **Neuroscience** 169(1): 39-51.

